Mathematical Models and Methods in Applied Sciences
(2020)

DOI: 10.1142/S0218202520500554



# An adaptive edge element approximation of a quasilinear $\boldsymbol{H}(\mathbf{curl})$-elliptic problem

Yifeng Xu

*Department of Mathematics,*
*Scientific Computing Key Laboratory of Shanghai Universities,*
*Shanghai Normal University, Shanghai 200234, P. R. China*
*yfxu@shnu.edu.cn*

Irwin Yousept*

*Fakultät für Mathematik, Universität Duisburg-Essen,*
*Thea-Leymann-Str. 9, Essen D-45127, Germany*
*irwin.yousept@uni-due.de*

Jun Zou

*Department of Mathematics,*
*The Chinese University of Hong Kong,*
*Shatin, N.T., Hong Kong*
*zou@math.cuhk.edu.hk*

Received 5 May 2020
Revised 21 September 2020
Accepted 30 September 2020
Published 10 December 2020
Communicated by F. Brezzi

An adaptive edge element method is designed to approximate a quasilinear $\boldsymbol{H}(\mathbf{curl})$-elliptic problem in magnetism, based on a residual-type *a posteriori* error estimator and general marking strategies. The error estimator is shown to be both reliable and efficient, and its resulting sequence of adaptively generated solutions converges strongly to the exact solution of the original quasilinear system. Numerical experiments are provided to verify the validity of the theoretical results.

*Keywords*: Quasilinear elliptic problem; Maxwell's equations; edge element; adaptive finite element method; convergence.

AMS Subject Classification: 65N12, 65N30, 35J62, 35Q60, 78M10

## 1. Introduction

We are interested in developing an adaptive finite element method (AFEM) for the numerical solution of the following nonlinear saddle point system, which arises from

*Corresponding author

the applications of ferromagnetic materials (see Refs. 3, 4, 28 and 42):

$$\begin{cases} \boldsymbol{\nabla} \times (\nu(\boldsymbol{x}, |\boldsymbol{\nabla} \times \boldsymbol{u}|)\boldsymbol{\nabla} \times \boldsymbol{u}) = \boldsymbol{f} & \text{in } \Omega, \\ \boldsymbol{\nabla} \cdot \boldsymbol{u} = g & \text{in } \Omega, \\ \boldsymbol{u} \times \boldsymbol{n} = \boldsymbol{0} & \text{on } \partial\Omega. \end{cases} \tag{1.1}$$

In this setting, $\boldsymbol{u}$ denotes a three-dimensional magnetic vector potential field, $\Omega \subset \mathbb{R}^3$ is a bounded polyhedral domain with a connected boundary $\partial\Omega$, $\boldsymbol{n}$ is the outward unit normal on $\partial\Omega$. Furthermore, the given source terms are $\boldsymbol{f} \in \boldsymbol{L}^2(\Omega)$ satisfying $\boldsymbol{\nabla} \cdot \boldsymbol{f} = 0$ and $g \in L^2(\Omega)$, which is often set to be zero in practical applications. The nonlinear reluctivity function $\nu : \Omega \times \mathbb{R}_0^+ \to \mathbb{R}$ is the inverse of the magnetic permeability where $\mathbb{R}_0^+$ denotes the set of all nonnegative numbers. We would like to mention that $\nu$ represents the nonlinear relation between the magnetic induction $\boldsymbol{B}$ and the magnetic field $\boldsymbol{H}$. In particular, this nonlinearity plays an important role in modeling of ferromagnetic materials (see Ref. 28). The precise mathematical properties of $\nu$ are stated in Sec. 2.

Edge elements (Ref. 32) are widely used in numerical simulation of Maxwell's equations thanks to its $\boldsymbol{H}(\mathbf{curl})$-conformity. There exist various numerical analyses in literature on the linearized problem associated with (1.1) (see Refs. 9, 13–15). More recently, a mathematical and numerical analysis was given in Ref. 42 for the optimal control of the quasilinear system (1.1). We should underline that, due to reentrant corners on $\partial\Omega$ and jumps of the nonlinear coefficient $\nu$ across interfaces of different media, local singularities are expected in the solution of (1.1) (see Refs. 16 and 17). Consequently, in terms of computing efficiency and accuracy, the classical uniform mesh refinement strategy is not efficient for solving (1.1). To improve numerical resolutions, AFEMs provide a promising effective tool. Based on an *a posteriori* error estimator, depending on the discrete solution, the mesh size and the given data, AFEM aims at producing a sequence of solutions with equidistributed error at minimum computational cost. Therefore, the interest of this paper lies in adaptive finite element approximations of (1.1). Generally speaking, a standard adaptive algorithm consists of the following successive loops:

$$\text{SOLVE} \to \text{ESTIMATE} \to \text{MARK} \to \text{REFINE}. \tag{1.2}$$

Here, SOLVE yields a finite element approximation on the current mesh; ESTIMATE measures the discretization error in some appropriate norm by a relevant *a posteriori* estimator; MARK selects some elements of the mesh to be subdivided; REFINE generates a finer new mesh by local refinement of all marked elements and their neighbors for conformity.

Since the seminal work by Babuška and Rheinboldt[2] in 1978, intensive developments have been made in the theory of AFEM over the past four decades (see Refs. 1 and 40 and the references therein). For edge element discretization of Maxwell's equations, we refer to Refs. 6, 9, 26, 35 and 46. The convergence of AFEM was first studied in Ref. 5 for a two-point boundary value problem, then in Ref. 19 for multi-dimensional problems. Over the past two decades, the theory of AFEM in

terms of convergence and decay rate has been widely investigated, e.g., for standard second-order elliptic problems Refs. 8, 31, 33 and 37 and for Maxwell system Refs. 11, 10, 20, 25, 37 and 47.

Although the theory of AFEM has reached a mature level for linear problems, the relevant study for nonlinear problems is still at an early stage. Existing works closely related to our current topic may be found in Refs. 7, 18, 22, 23 and 39 for quasilinear elliptic problems of $p$-Laplacian and strongly monotone type.

This paper is concerned with AFEM for the quasilinear saddle point magnetostatic Maxwell system (1.1). We propose a residual-type *a posteriori* error estimator consisting of element and face residuals associated with the discrete system of (1.1) on the basis of the lowest order edge elements of Nédélec's first family.[32] Compared with existing works for nonlinear elliptic problems, the great difficulty in the current *a posteriori* error analysis lies in the saddle point structure and the nonlinear curl-curl operator in (1.1). With several crucial and delicate analytical strategies, we are still able to establish both the reliability and efficiency of the estimator (Theorems 3.1 and 3.2) for this nonlinear Maxwell system. More specifically, our basic analysis makes a full use of the nonlinear properties of the reluctivity function $\nu$ (cf. (2.2)–(2.5)), an equivalent norm on the admissible space (Remark 2.1) and the Schöberl quasi-interpolation operator[35] (Lemma 3.1). An adaptive algorithm of the form (1.2) is proposed and proved to ensure the $\boldsymbol{H}(\mathbf{curl})$-strong convergence of the adaptive discrete solutions towards the solution of (1.1) (Theorem 5.2) and a vanishing limit of the sequence of error estimators (Theorem 5.3). Our convergence analysis relies on a limiting saddle point problem resulting from adaptively generated edge element spaces; see (5.3). We show the $\boldsymbol{H}(\mathbf{curl})$-strong convergence of the adaptive discrete solutions towards the solution of the limiting problem (Theorem 5.1). Then, with the help of some existing techniques, we prove in Lemma 5.3 that the limiting solution satisfies (1.1), which in turn yields the desired $\boldsymbol{H}(\mathbf{curl})$-strong convergence of the adaptive discrete solutions (Theorem 5.2). The convergence result for the sequence of error estimators (Theorem 5.3) is the consequence of Theorem 5.2 and the efficiency of the estimator.

We would like to make a further remark now about our main analysis in this work. We follow basically the general analytical strategy for elliptic problems, but there are several essential technical differences here due to the saddle point structure and the nonlinearity of $\nu$. For linear/nonlinear elliptic operators, the relevant limiting space required in the convergence of adaptive methods is a proper subspace of the corresponding admissible space, e.g. $H^1(\Omega)$, many properties for the limiting variational system are inherited automatically from the standard variational theory, particularly, the unique solvability of the limiting problem. However, this is not trivial for the current nonlinear saddle point Maxwell problem because the related continuous space $\boldsymbol{X}$ (see Sec. 2) does not contain the limiting space $\boldsymbol{X}_\infty$ (see Sec. 5) on which the coercivity is required. We shall resort to a Poincaré-type inequality (5.2) over $\boldsymbol{X}_\infty$ to overcome the difficulty. Further, a general approach to establish a Cea-type lemma, which may directly lead to an auxiliary strong convergence as

stated in Theorem 5.1 in the case of elliptic problems, now fails due to the divergence constraint in (1.1). This key component is now achieved by making use of some elegant techniques from mixed element methods.

The rest of this paper is organized as follows. In Sec. 2, we briefly describe the variational formulation of (1.1) and its discretization based on the lowest order edge elements of Nédélec's first family.[32] Section 3 is devoted to reliability and efficiency of a residual-based *a posteriori* error estimator, with the help of which, we propose an adaptive algorithm in Sec. 4. The convergence analysis is conducted in Sec. 5. Finally, we present numerical results as an illustration of our theoretical findings in Sec. 6.

Throughout this paper, we adopt the standard notation for the Lebesgue space $L^\infty(G)$ and Sobolev spaces $W^{m,p}(G)$ for real number $m$ on an open bounded set $G \subset \mathbb{R}^3$. Related norms and semi-norms of $H^m(G)$ $(p = 2)$ as well as the norm of $L^\infty(G)$ are denoted by $\|\cdot\|_{m,G}$, $|\cdot|_{m,G}$ and $\|\cdot\|_{L^\infty(G)}$, respectively. We use $(\cdot,\cdot)_G$ to denote the $L^2(G)$ scalar product, and the subscript is omitted when $G = \Omega$. Moreover, we shall use $C$, with or without subscript, for a generic constant independent of the mesh size, and it may take a different value at each occurrence.

## 2. Variational Formulation

We first introduce some Hilbert spaces, operators and assumptions, which are required in the subsequent analysis:

$$\begin{aligned}
\boldsymbol{H}(\mathbf{curl}) &= \{\boldsymbol{v} \in \boldsymbol{L}^2(\Omega) \,|\, \boldsymbol{\nabla} \times \boldsymbol{v} \in \boldsymbol{L}^2(\Omega)\},\\
\boldsymbol{H}_0(\mathbf{curl}) &= \{\boldsymbol{v} \in \boldsymbol{H}(\mathbf{curl}) \,|\, \gamma_t(\boldsymbol{v}) = 0\},\\
\boldsymbol{X} &= \{\boldsymbol{v} \in \boldsymbol{H}_0(\mathbf{curl}) \,|\, (\boldsymbol{v}, \boldsymbol{\nabla} q) = 0 \quad \forall\, q \in H_0^1(\Omega)\},
\end{aligned}$$

where the **curl**-operator is understood in the distributional sense, and $\gamma_t : \boldsymbol{H}(\mathbf{curl}) \to \boldsymbol{H}^{-\frac{1}{2}}(\partial\Omega)$ denotes the tangential trace (see Ref. 24). We focus on the standard mixed variational formulation for (1.1): Find $(\boldsymbol{u}, p) \in \boldsymbol{H}_0(\mathbf{curl}) \times H_0^1(\Omega)$ such that

$$\begin{cases} (\nu(\boldsymbol{x}, |\boldsymbol{\nabla} \times \boldsymbol{u}|)\boldsymbol{\nabla} \times \boldsymbol{u}, \boldsymbol{\nabla} \times \boldsymbol{v}) + (\boldsymbol{v}, \boldsymbol{\nabla} p) = (\boldsymbol{f}, \boldsymbol{v}) & \forall\, \boldsymbol{v} \in \boldsymbol{H}_0(\mathbf{curl}),\\ (\boldsymbol{u}, \boldsymbol{\nabla} q) = -(g, q) & \forall\, q \in H_0^1(\Omega). \end{cases} \tag{2.1}$$

Our numerical analysis relies on the following regularity assumptions for the nonlinear reluctivity function $\nu : \Omega \times \mathbb{R}_0^+ \to \mathbb{R}$. We should underline that these assumptions are physically reasonable and typically considered for the mathematical model of ferromagnetic materials (cf. Refs. 3, 4 and 28).

**Assumption 2.1 (Regularity assumption for $\nu : \Omega \times \mathbb{R}_0^+ \to \mathbb{R}$).** (i) For every $s \in \mathbb{R}_0^+$, the function $\nu(\cdot, s) : \Omega \to \mathbb{R}$ is measurable.

(ii) For almost all $\boldsymbol{x} \in \Omega$, the function $\nu(\boldsymbol{x}, \cdot) : \mathbb{R}_0^+ \to \mathbb{R}$ is continuous. For every piecewise constant $\boldsymbol{y} \in \boldsymbol{L}^1(\Omega)$, the function $\nu(\cdot, |\boldsymbol{y}(\cdot)|) : \Omega \to \mathbb{R}$ is piecewise $W^{1,\infty}$.

(iii) There exist positive constants $\nu_1$ and $\nu_2$ such that

$$\lim_{s\to\infty} \nu(\boldsymbol{x}, s) = \nu_2 \quad \text{for almost all } \boldsymbol{x} \in \Omega, \tag{2.2}$$

$$\nu_1 \le \nu(\boldsymbol{x}, s) \le \nu_2 \quad \text{for almost all } \boldsymbol{x} \in \Omega \text{ and all } s \ge 0, \tag{2.3}$$

$$(\nu(\boldsymbol{x}, s)s - \nu(\boldsymbol{x}, t)t)(s - t) \ge \nu_1 |s - t|^2 \quad \forall\, s, t \ge 0 \text{ and almost all } \boldsymbol{x} \in \Omega. \tag{2.4}$$

(iv) There exists a constant $\bar{\nu} \in [\nu_2, \infty)$ such that

$$|\nu(\boldsymbol{x}, s)s - \nu(\boldsymbol{x}, t)t| \le \bar{\nu}|s - t| \quad \forall\, s, t \ge 0 \text{ and almost all } \boldsymbol{x} \in \Omega. \tag{2.5}$$

We shall often need an operator $A : \boldsymbol{H}_0(\mathbf{curl}) \to \boldsymbol{H}_0(\mathbf{curl})^*$ defined by

$$\langle A\boldsymbol{v}, \hat{\boldsymbol{v}}\rangle := (\nu(\boldsymbol{x}, |\boldsymbol{\nabla} \times \boldsymbol{v}|)\boldsymbol{\nabla} \times \boldsymbol{v}, \boldsymbol{\nabla} \times \hat{\boldsymbol{v}}) \quad \forall\, \boldsymbol{v}, \hat{\boldsymbol{v}} \in \boldsymbol{H}_0(\mathbf{curl}).$$

As shown in Lemma 2.2 of Ref. 42, (2.4) and (2.5) imply that

$$\langle A\boldsymbol{v} - A\hat{\boldsymbol{v}}, \boldsymbol{v} - \hat{\boldsymbol{v}}\rangle \ge \nu_1 \|\boldsymbol{\nabla} \times (\boldsymbol{v} - \hat{\boldsymbol{v}})\|_0^2 \quad \forall\, \boldsymbol{v}, \hat{\boldsymbol{v}} \in \boldsymbol{H}_0(\mathbf{curl}), \tag{2.6}$$

$$|\langle A\boldsymbol{v} - A\hat{\boldsymbol{v}}, \boldsymbol{w}\rangle| \le L\|\boldsymbol{\nabla} \times (\boldsymbol{v} - \hat{\boldsymbol{v}})\|_0 \|\boldsymbol{\nabla} \times \boldsymbol{w}\|_0 \quad \forall\, \boldsymbol{v}, \hat{\boldsymbol{v}}, \boldsymbol{w} \in \boldsymbol{H}_0(\mathbf{curl}), \tag{2.7}$$

with $L = 2\nu_1 + \bar{\nu}$. Thus, by virtue of the Poincaré-type inequality (see Ref. 27)

$$\|\boldsymbol{v}\|_0 \le C\|\boldsymbol{\nabla} \times \boldsymbol{v}\|_0 \quad \forall\, \boldsymbol{v} \in \boldsymbol{X}, \tag{2.8}$$

(2.6) implies that $A : \boldsymbol{H}_0(\mathbf{curl}) \to \boldsymbol{H}_0(\mathbf{curl})^*$ is strongly monotone on $\boldsymbol{X}$; i.e.

$$\langle A\boldsymbol{v} - A\hat{\boldsymbol{v}}, \boldsymbol{v} - \hat{\boldsymbol{v}}\rangle \ge C_M \|\boldsymbol{v} - \hat{\boldsymbol{v}}\|_{\boldsymbol{H}(\mathbf{curl})}^2 \quad \forall\, \boldsymbol{v}, \hat{\boldsymbol{v}} \in \boldsymbol{X}, \tag{2.9}$$

with a constant $C_M > 0$ depending only on $\nu_1$ and $\Omega$. Moreover, it is well known that the inf-sup condition

$$\sup_{\mathbf{0} \ne \boldsymbol{v} \in \boldsymbol{H}_0(\mathbf{curl})} \frac{(\boldsymbol{v}, \boldsymbol{\nabla} q)}{\|\boldsymbol{v}\|_{\boldsymbol{H}(\mathbf{curl})}} \ge C\|q\|_1 \quad \forall\, q \in H_0^1(\Omega) \tag{2.10}$$

is satisfied with a constant $C > 0$ depending only on $\Omega$. As a consequence of (2.7), (2.9) and (2.10), the problem (2.1) admits a unique solution (Proposition 23 in Ref. 34), and there exists a positive constant $C$, independent of $\boldsymbol{u}$, $\boldsymbol{f}$ and $g$, such that

$$\|\boldsymbol{u}\|_{\boldsymbol{H}(\mathbf{curl})} \le C(\|\boldsymbol{f}\|_0 + \|g\|_0).$$

We note that, since $\boldsymbol{\nabla} \cdot \boldsymbol{f} = 0$, inserting $\boldsymbol{v} = \boldsymbol{\nabla}\phi$ into the first equation of (2.1) implies that the Lagrangian multiplier vanishes, i.e. $p \equiv 0$.

**Remark 2.1.** A direct consequence of (2.8) is that $\|\boldsymbol{\nabla} \times \cdot\|_0$ is equivalent to the graph norm on $\boldsymbol{X}$. Noting that $\boldsymbol{X}$ and $\boldsymbol{\nabla} H_0^1(\Omega)$ are $L^2$-orthogonal and $\boldsymbol{H}_0(\mathbf{curl}) = \boldsymbol{X} \oplus \boldsymbol{\nabla} H_0^1(\Omega)$ (see Ref. 27), we may define an alternative norm equivalent to the graph one on $\boldsymbol{H}_0(\mathbf{curl})$, namely, $(\|\boldsymbol{\nabla} \times \boldsymbol{v}\|_0^2 + \|\boldsymbol{v}^0\|_0^2)^{1/2}$, where $\boldsymbol{v}^0$ is the $L^2$-projection of $\boldsymbol{v}$ on $\boldsymbol{\nabla} H_0^1(\Omega)$.

Let us now consider the discrete approximation of the problem (2.1). Let $\mathcal{T}_0$ be a shape regular conforming triangulation of $\overline{\Omega}$ into closed tetrahedra such that for every piecewise constant function $\boldsymbol{y}$ over $\mathcal{T}_0$, the function $\nu(\cdot, |\boldsymbol{y}(\cdot)|) : \Omega \to \mathbb{R}_0^+$ is piecewise $W^{1,\infty}$ over $\mathcal{T}_0$, and $\mathbb{T}$ be the set of all possible conforming triangulations obtained from $\mathcal{T}_0$ by successive bisections (see Refs. 29 and 33). One key property of the refinement process ensures that all constants depending on the shape regularity of any $\mathcal{T} \in \mathbb{T}$ are uniformly bounded by a constant only depending on the initial mesh $\mathcal{T}_0$ (see Refs. 33 and 38). Then, for any $\mathcal{T} \in \mathbb{T}$, we introduce the lowest order edge elements of Nédélec's first family[32]

$$\boldsymbol{V}_{\mathcal{T}} = \{\boldsymbol{v} \in \boldsymbol{H}_0(\mathbf{curl}) \,|\, \boldsymbol{v}|_T = \boldsymbol{a}_T + \boldsymbol{b}_T \times \boldsymbol{x} \; \boldsymbol{a}_T, \boldsymbol{b}_T \in \mathbb{R}^3 \; \forall T \in \mathcal{T}\}.$$

For the numerical treatment of the Lagrange multiplier, we also need the standard piecewise linear finite element space $S_{\mathcal{T}} \subset H_0^1(\Omega)$, for which we know the following inclusion relation (Ref. 27):

$$\boldsymbol{\nabla} S_{\mathcal{T}} \subset \boldsymbol{V}_{\mathcal{T}}. \tag{2.11}$$

The discrete problem of (2.1) is now formulated: Find $(\boldsymbol{u}_{\mathcal{T}}, p_{\mathcal{T}}) \in \boldsymbol{V}_{\mathcal{T}} \times S_{\mathcal{T}}$ such that

$$\begin{cases} (\nu(\boldsymbol{x}, |\boldsymbol{\nabla} \times \boldsymbol{u}_{\mathcal{T}}|)\boldsymbol{\nabla} \times \boldsymbol{u}_{\mathcal{T}}, \boldsymbol{\nabla} \times \boldsymbol{v}_{\mathcal{T}}) + (\boldsymbol{v}_{\mathcal{T}}, \boldsymbol{\nabla} p_{\mathcal{T}}) = (\boldsymbol{f}, \boldsymbol{v}_{\mathcal{T}}) \quad \forall \boldsymbol{v}_{\mathcal{T}} \in \boldsymbol{V}_{\mathcal{T}}, \\ (\boldsymbol{u}_{\mathcal{T}}, \boldsymbol{\nabla} q_{\mathcal{T}}) = -(g, q_{\mathcal{T}}) \quad \forall \; q_{\mathcal{T}} \in S_{\mathcal{T}}. \end{cases} \tag{2.12}$$

As in the continuous case, the unique solvability of the discrete problem (2.12) is also true by virtue of Proposition 2.3 in Ref. 34, (2.6), (2.7), the discrete Poincaré-type inequality and the discrete inf–sup condition (see Refs. 9 and 27)

$$\|\boldsymbol{v}_{\mathcal{T}}\|_0 \le C\|\boldsymbol{\nabla} \times \boldsymbol{v}_{\mathcal{T}}\|_0 \quad \forall \; \boldsymbol{v}_{\mathcal{T}} \in \boldsymbol{X}_{\mathcal{T}}, \tag{2.13}$$

$$\sup_{\mathbf{0} \neq \boldsymbol{v}_{\mathcal{T}} \in \boldsymbol{V}_{\mathcal{T}}} \frac{(\boldsymbol{v}_{\mathcal{T}}, \boldsymbol{\nabla} q_{\mathcal{T}})}{\|\boldsymbol{v}_{\mathcal{T}}\|_{\boldsymbol{H}(\mathbf{curl})}} \ge \|\boldsymbol{\nabla} q_{\mathcal{T}}\|_0 \quad \forall \; q_{\mathcal{T}} \in S_{\mathcal{T}}, \tag{2.14}$$

where the constant only depends on $\Omega$ and the shape-regularity of $\mathcal{T}$, and

$$\boldsymbol{X}_{\mathcal{T}} := \{\boldsymbol{v}_{\mathcal{T}} \in \boldsymbol{V}_{\mathcal{T}} \mid (\boldsymbol{v}_{\mathcal{T}}, \boldsymbol{\nabla} q_{\mathcal{T}}) = 0 \; \forall \; q_{\mathcal{T}} \in S_{\mathcal{T}}\}.$$

Moreover, there also holds the following stability result:

$$\|\boldsymbol{u}_{\mathcal{T}}\|_{\boldsymbol{H}(\mathbf{curl})} \le C(\|\boldsymbol{f}\|_0 + \|g\|_0).$$

The inclusion (2.11) allows $\boldsymbol{v}_{\mathcal{T}} = \boldsymbol{\nabla} \phi_{\mathcal{T}}$ in the first equation of (2.12). Then as in the continuous case, thanks to $\boldsymbol{\nabla} \cdot \boldsymbol{f} = 0$ the Lagrangian multiplier $p_{\mathcal{T}}$ also vanishes.

## 3. *A Posteriori* Error Estimate

This section deals with reliability and efficiency of a residual-type error estimator for the problem (2.12). For this purpose, some more notation and definitions are needed. The diameter of $T \in \mathcal{T}$ is denoted by $h_T := |T|^{1/3}$. The collection of all faces (resp. all interior faces) in $\mathcal{T}$ is denoted by $\mathcal{F}_{\mathcal{T}}$ (resp. $\mathcal{F}_{\mathcal{T}}(\Omega)$). The scalar $h_F := |F|^{1/2}$

stands for the diameter of $F \in \mathcal{F}_{\mathcal{T}}$, which is associated with a fixed normal unit vector $\boldsymbol{n}_F$ in $\overline{\Omega}$ with $\boldsymbol{n}_F = \boldsymbol{n}$ on the boundary $\partial\Omega$. We use $D_T$ (respectively, $D_F$) for the union of all elements in $\mathcal{T}$ with non-empty intersection with element $T \in \mathcal{T}$ (respectively, $F \in \mathcal{F}_{\mathcal{T}}$). Furthermore, for any $T \in \mathcal{T}$ (respectively, $F \in \mathcal{F}_{\mathcal{T}}$) we denote by $\omega_T$ (respectively, $\omega_F$) the union of elements in $\mathcal{T}$ sharing a common face with $T$ (respectively, with $F$ as a face).

For the solution $\boldsymbol{u}_{\mathcal{T}}$ to the problem (2.12), we define an element residual on any $T \in \mathcal{T}$ by

$$\boldsymbol{R}_T := \boldsymbol{f} - \boldsymbol{\nabla} \times (\nu(\cdot, |\boldsymbol{\nabla} \times \boldsymbol{u}_{\mathcal{T}}|)\boldsymbol{\nabla} \times \boldsymbol{u}_{\mathcal{T}}),$$

and two jumps across $F \in \mathcal{F}_{\mathcal{T}}(\Omega)$

$$\boldsymbol{J}_{F,1} := [(\nu(\cdot, |\boldsymbol{\nabla} \times \boldsymbol{u}_{\mathcal{T}}|)\boldsymbol{\nabla} \times \boldsymbol{u}_{\mathcal{T}}) \times \boldsymbol{n}_F], \quad J_{F,2} := [\boldsymbol{u}_{\mathcal{T}} \cdot \boldsymbol{n}_F].$$

For any $\mathcal{M} \subseteq \mathcal{T}$, we introduce the estimator

$$\eta_{\mathcal{T}}^2(\boldsymbol{u}_{\mathcal{T}}, \boldsymbol{f}, g, \mathcal{M}) := \eta_{\mathcal{T},1}^2(\boldsymbol{u}_{\mathcal{T}}, \boldsymbol{f}, \mathcal{M}) + \eta_{\mathcal{T},2}^2(\boldsymbol{u}_{\mathcal{T}}, g, \mathcal{M}), \tag{3.1}$$

$$\begin{aligned}\eta_{\mathcal{T},1}^2(\boldsymbol{u}_{\mathcal{T}}, \boldsymbol{f}, \mathcal{M}) &:= \sum_{T\in\mathcal{M}} \eta_{\mathcal{T},1}^2(\boldsymbol{u}_{\mathcal{T}}, \boldsymbol{f}, T) \\ &= \sum_{T\in\mathcal{M}} \left( h_T^2 \|\boldsymbol{R}_T\|_{0,T}^2 + \sum_{F\in\partial T\cap\Omega} h_F \|\boldsymbol{J}_{F,1}\|_{0,F}^2 \right),\end{aligned} \tag{3.2}$$

$$\begin{aligned}\eta_{\mathcal{T},2}^2(\boldsymbol{u}_{\mathcal{T}}, g, \mathcal{M}) &:= \sum_{T\in\mathcal{M}} \eta_{\mathcal{T},2}^2(\boldsymbol{u}_{\mathcal{T}}, g, T) \\ &= \sum_{T\in\mathcal{M}} \left( h_T^2 \|g\|_{0,T}^2 + \sum_{F\in\partial T\cap\Omega} h_F \|J_{F,2}\|_{0,F}^2 \right),\end{aligned} \tag{3.3}$$

and the oscillation term $\operatorname{osc}_{\mathcal{T}}^2(\boldsymbol{u}_{\mathcal{T}}, f, g, \mathcal{M}) := \sum_{T\in\mathcal{M}} \operatorname{osc}_{\mathcal{T}}^2(\boldsymbol{u}, f, g, T)$ with

$$\begin{aligned}\operatorname{osc}_{\mathcal{T}}^2(\boldsymbol{u}, f, g, T) := h_T^2 \|\boldsymbol{R}_T - \overline{\boldsymbol{R}}_T\|_{0,T}^2 + h_T^2 \|g - \overline{g}_T\|_{0,T}^2 \\ + \sum_{F\in\partial T\cap\Omega} h_F \|\boldsymbol{J}_{F,1} - \overline{\boldsymbol{J}}_{F,1}\|_{0,F}^2,\end{aligned}$$

where $\overline{\boldsymbol{R}}_T$, $\overline{g}_T$ and $\overline{\boldsymbol{J}}_{F,1}$ are the averages of $\boldsymbol{R}_T$, $g$ and $\boldsymbol{J}_{F,1}$ over $T$ and $F$, respectively, namely $\overline{\boldsymbol{R}}_T = \int_T \boldsymbol{R}_T dx/|T|$, $\overline{g}_T = \int_T g dx/|T|$ and $\overline{\boldsymbol{J}}_{F,1} = \int_F \boldsymbol{J}_{F,1} ds/|F|$. For simplicity, if $\mathcal{M} = \mathcal{T}$ we often write

$$\eta_{\mathcal{T}}(\boldsymbol{u}_{\mathcal{T}}, \boldsymbol{f}, g) = \eta_{\mathcal{T}}(\boldsymbol{u}_{\mathcal{T}}, \boldsymbol{f}, g, \mathcal{T}).$$

To relate functions in $\boldsymbol{H}_0(\mathbf{curl})$ and $H_0^1(\Omega)$ to discrete spaces $\boldsymbol{V}_{\mathcal{T}}$ and $S_{\mathcal{T}}$, respectively, we need a quasi-interpolation operator $I_{\mathcal{T}}^{sz} : H_0^1(\Omega) \to S_{\mathcal{T}}$ (Ref. 36)

$$\|q - I_{\mathcal{T}}^{sz} q\|_{0,T} \le C h_T |q|_{1,D_T}, \quad \|q - I_{\mathcal{T}}^{sz} q\|_{0,F} \le C h_F^{1/2} |q|_{1,D_F} \quad \forall\ q \in H_0^1(\Omega). \tag{3.4}$$

and the following local regular decomposition (see Theorem 1 in Ref. 35).

**Lemma 3.1.** *There exists a quasi-interpolation operator* $\boldsymbol{\Pi}_{\mathcal{T}}^s : \boldsymbol{H}_0(\mathbf{curl}) \to \boldsymbol{V}_{\mathcal{T}}$ *such that for every* $\boldsymbol{v} \in \boldsymbol{H}_0(\mathbf{curl})$ *there exist* $\boldsymbol{z} \in \boldsymbol{H}_0^1(\Omega)$ *and* $\varphi \in H_0^1(\Omega)$ *satisfying*

$$\boldsymbol{v} - \boldsymbol{\Pi}_{\mathcal{T}}^s \boldsymbol{v} = \boldsymbol{z} + \boldsymbol{\nabla}\varphi, \tag{3.5}$$

*with the stability estimates*

$$h_T^{-1}\|\boldsymbol{z}\|_{0,T} + |\boldsymbol{z}|_{1,T} \le C\|\boldsymbol{\nabla}\times\boldsymbol{v}\|_{0,\widetilde{D}_T}, \quad h_T^{-1}\|\varphi\|_{0,T} + |\varphi|_{1,T} \le C\|\boldsymbol{v}\|_{0,\widetilde{D}_T}, \tag{3.6}$$

*where constant* $C$ *depends only on the shape of the elements in the enlarged element patch* $\widetilde{D}_T := \cup\{T' \in \mathcal{T} \mid T' \cap D_T \neq \emptyset\}$, *not on the global shape of domain* $\Omega$ *or the size of* $\widetilde{D}_T$.

We are now in a position to establish the reliability of the estimator in (3.1) for the error $\boldsymbol{u} - \boldsymbol{u}_{\mathcal{T}}$ in $\boldsymbol{H}(\mathbf{curl})$-norm.

**Theorem 3.1.** *Let* $\boldsymbol{u}$ *and* $\boldsymbol{u}_{\mathcal{T}}$ *be solutions of problems* (2.1) *and* (2.12), *respectively. Then there exists a constant* $C > 0$, *depending on* $\nu_1$, $\Omega$ *and the shape-regularity of* $\mathcal{T}$, *such that*

$$\|\boldsymbol{u} - \boldsymbol{u}_{\mathcal{T}}\|_{\boldsymbol{H}(\mathbf{curl})}^2 \le C\eta_{\mathcal{T}}^2(\boldsymbol{u}_{\mathcal{T}}, \boldsymbol{f}, g). \tag{3.7}$$

**Proof.** By virtue of (2.6) and $p = p_{\mathcal{T}} = 0$, we take $\boldsymbol{v} = \boldsymbol{u} - \boldsymbol{u}_{\mathcal{T}}$ in the first equation of (2.1), apply Lemma 3.1 with $\boldsymbol{v} - \boldsymbol{\Pi}_{\mathcal{T}}^s\boldsymbol{v} = \boldsymbol{z} + \boldsymbol{\nabla}\varphi$, use the first equation of (2.12), and perform an elementwise integration by parts to deduce that

$$\begin{aligned}
\nu_1\|\boldsymbol{\nabla}\times(\boldsymbol{u}-\boldsymbol{u}_{\mathcal{T}})\|_0^2 &\le \langle A\boldsymbol{u} - A\boldsymbol{u}_{\mathcal{T}}, \boldsymbol{u} - \boldsymbol{u}_{\mathcal{T}}\rangle \\
&= (\boldsymbol{f}, \boldsymbol{u} - \boldsymbol{u}_{\mathcal{T}}) - (\nu(\cdot, |\boldsymbol{\nabla}\times\boldsymbol{u}_{\mathcal{T}}|)\boldsymbol{\nabla}\times\boldsymbol{u}_{\mathcal{T}}, \boldsymbol{\nabla}\times(\boldsymbol{u}-\boldsymbol{u}_{\mathcal{T}})) \\
&= (\boldsymbol{f}, \boldsymbol{v} - \boldsymbol{\Pi}_{\mathcal{T}}^s\boldsymbol{v}) - (\nu(\cdot, |\boldsymbol{\nabla}\times\boldsymbol{u}_{\mathcal{T}}|)\boldsymbol{\nabla}\times\boldsymbol{u}_{\mathcal{T}}, \\
&\quad \boldsymbol{\nabla}\times(\boldsymbol{v} - \boldsymbol{\Pi}_{\mathcal{T}}^s\boldsymbol{v})) \\
&= (\boldsymbol{f}, \boldsymbol{z} + \boldsymbol{\nabla}\varphi) - (\nu(\cdot, |\boldsymbol{\nabla}\times\boldsymbol{u}_{\mathcal{T}}|)\boldsymbol{\nabla}\times\boldsymbol{u}_{\mathcal{T}}, \boldsymbol{\nabla}\times\boldsymbol{z}) \\
&\underbrace{=}_{\boldsymbol{\nabla}\cdot\boldsymbol{f}=0} (\boldsymbol{f}, \boldsymbol{z}) - (\nu(\cdot, |\boldsymbol{\nabla}\times\boldsymbol{u}_{\mathcal{T}}|)\boldsymbol{\nabla}\times\boldsymbol{u}_{\mathcal{T}}, \boldsymbol{\nabla}\times\boldsymbol{z}) \\
&= \sum_{T\in\mathcal{T}} (\boldsymbol{R}_T, \boldsymbol{z})_T - \sum_{F\in\mathcal{F}_{\mathcal{T}}(\Omega)} (\boldsymbol{J}_{F,1}, \boldsymbol{z})_F \\
&\le \sum_{T\in\mathcal{T}} h_T\|\boldsymbol{R}_T\|_{0,T} h_T^{-1}\|\boldsymbol{z}\|_{0,T} \\
&\quad + \sum_{F\in\mathcal{F}_{\mathcal{T}}(\Omega)} h_T^{1/2}\|\boldsymbol{J}_{F,1}\|_{0,T} h_F^{-1/2}\|\boldsymbol{z}\|_{0,F} \\
&\le C\sum_{T\in\mathcal{T}} \eta_{\mathcal{T},1}(\boldsymbol{u}_{\mathcal{T}}, \boldsymbol{f}, T)(h_T^{-1}\|\boldsymbol{z}\|_{0,T} + |\boldsymbol{z}|_{1,T})
\end{aligned}$$

$$\underbrace{\leq}_{(3.6)} C\sum_{T\in\mathcal{T}}\eta_{\mathcal{T},1}(\boldsymbol{u}_{\mathcal{T}},\boldsymbol{f},T)\|\boldsymbol{\nabla}\times(\boldsymbol{u}-\boldsymbol{u}_{\mathcal{T}})\|_{0,\widetilde{D}_T}.$$

(by the trace theorem; Ref. 40)

Hence, it follows from the finite overlapping property of the patches $\widetilde{D}_T$ that

$$\|\boldsymbol{\nabla}\times(\boldsymbol{u}-\boldsymbol{u}_{\mathcal{T}})\|_0 \leq C\eta_{\mathcal{T},1}(\boldsymbol{u}_{\mathcal{T}},\boldsymbol{f}). \tag{3.8}$$

On the other hand, we make use of the error estimate (3.4) for the quasi-interpolation operator $I_{\mathcal{T}}^{sz}$ and the fact that $\boldsymbol{\nabla}\cdot\boldsymbol{u}_{\mathcal{T}}=0$ on each $T\in\mathcal{T}$ to deduce from the second equation of (2.1) and (2.12) that

$$\begin{aligned}(\boldsymbol{u}-\boldsymbol{u}_{\mathcal{T}},\boldsymbol{\nabla}q) &= -(g,q)-(\boldsymbol{u}_{\mathcal{T}},\boldsymbol{\nabla}q) = -(g,q-I_{\mathcal{T}}^{sz}q)-(\boldsymbol{u}_{\mathcal{T}},\boldsymbol{\nabla}(q-I_{\mathcal{T}}^{sz}q))\\ &= \sum_{T\in\mathcal{T}}(-g,q-I_{\mathcal{T}}^{sz}q)_T-\sum_{F\in\mathcal{F}_{\mathcal{T}}(\Omega)}(J_{F,2},q-I_{\mathcal{T}}^{sz}q)_F\\ &\leq C\eta_{\mathcal{T},2}(\boldsymbol{u}_{\mathcal{T}},g)|q|_1 \quad \forall\, q\in H_0^1(\Omega)\,,\end{aligned}$$

which implies

$$(\boldsymbol{u}-\boldsymbol{u}_{\mathcal{T}},(\boldsymbol{u}-\boldsymbol{u}_{\mathcal{T}})^0)\leq C\eta_{\mathcal{T},2}(\boldsymbol{u}_{\mathcal{T}},g)\|(\boldsymbol{u}-\boldsymbol{u}_{\mathcal{T}})^0\|_0,$$

where $(\boldsymbol{u}-\boldsymbol{u}_{\mathcal{T}})^0$ is the $L^2$-projection of $\boldsymbol{u}-\boldsymbol{u}_{\mathcal{T}}$ on $\boldsymbol{\nabla}H_0^1(\Omega)$. This clearly shows

$$\|(\boldsymbol{u}-\boldsymbol{u}_{\mathcal{T}})^0\|_0\leq C\eta_{\mathcal{T},2}(\boldsymbol{u}_{\mathcal{T}},g). \tag{3.9}$$

A collection of (3.8), (3.9) and the norm equivalence in Remark 2.1 leads to the desired estimate. □

We end this section by showing that the estimator in (3.1) is also efficient for the error $\boldsymbol{u}-\boldsymbol{u}_{\mathcal{T}}$ in $\boldsymbol{H}(\mathbf{curl})$-norm.

**Theorem 3.2.** *Let* $\boldsymbol{u}$ *and* $\boldsymbol{u}_{\mathcal{T}}$ *be solutions of problems* (2.1) *and* (2.12)*, respectively. Then there exists a constant* $C>0$*, depending on* $L$*, the Lipschitz constant in* (2.7)*, and the shape-regularity of* $\mathcal{T}$*, such that*

$$\eta_{\mathcal{T}}^2(\boldsymbol{u}_{\mathcal{T}},\boldsymbol{f},g,T)\leq C(\|\boldsymbol{u}-\boldsymbol{u}_{\mathcal{T}}\|^2_{\boldsymbol{H}(\mathbf{curl};\omega_T)}+\mathrm{osc}_{\mathcal{T}}^2(\boldsymbol{f},g,\omega_T))\quad\forall\, T\in\mathcal{T}. \tag{3.10}$$

**Proof.** For any given $T\in\mathcal{T}$, let $b_T$ be the usual tetrahedral bubble function on $T$ (see Ref. 40). With $\boldsymbol{v}=\boldsymbol{v}_T=\overline{\boldsymbol{R}}_T b_T\in\boldsymbol{H}_0^1(T)$ and $p\equiv 0$ in the first equation of (2.1), the standard scaling argument, the definition of $\boldsymbol{R}_T$ and integration by parts imply

$$\begin{aligned}C\|\overline{\boldsymbol{R}}_T\|_{0,T}^2 &\leq (\overline{\boldsymbol{R}}_T,\boldsymbol{v}_T)_T=(\overline{\boldsymbol{R}}_T-\boldsymbol{R}_T,\boldsymbol{v}_T)_T+(\boldsymbol{R}_T,\boldsymbol{v}_T)_T\\ &= (\boldsymbol{f}-\boldsymbol{\nabla}\times(\nu(\cdot,|\boldsymbol{\nabla}\times\boldsymbol{u}_{\mathcal{T}}|)\boldsymbol{\nabla}\times\boldsymbol{u}_{\mathcal{T}}),\boldsymbol{v}_T)_T+(\overline{\boldsymbol{R}}_T-\boldsymbol{R}_T,\boldsymbol{v}_T)_T\end{aligned}$$

$$
\begin{aligned}
&= (\nu(\cdot,|\boldsymbol{\nabla}\times\boldsymbol{u}|)\boldsymbol{\nabla}\times\boldsymbol{u} - \nu(\cdot,|\boldsymbol{\nabla}\times\boldsymbol{u}_{\mathcal{T}}|)\boldsymbol{\nabla}\times\boldsymbol{u}_{\mathcal{T}}, \boldsymbol{\nabla}\times\boldsymbol{v}_T)_T \\
&\quad + (\overline{\boldsymbol{R}}_T - \boldsymbol{R}_T, \boldsymbol{v}_T)_T \\
&\le L\|\boldsymbol{u}-\boldsymbol{u}_{\mathcal{T}}\|_{\boldsymbol{H}(\mathbf{curl};T)}\|\boldsymbol{v}_T\|_{\boldsymbol{H}(\mathbf{curl};T)} + \|\boldsymbol{R}_T - \overline{\boldsymbol{R}}_T\|_{0,T}\|\boldsymbol{v}_T\|_{0,T},
\end{aligned}
$$

which, together with the inverse estimate, the scaling argument and the triangle inequality, yields

$$
Ch_T^2\|\boldsymbol{R}_T\|_{0,T}^2 \le \|\boldsymbol{u}-\boldsymbol{u}_{\mathcal{T}}\|_{\boldsymbol{H}(\mathbf{curl}),T}^2 + h_T^2\|\boldsymbol{R}_T - \overline{\boldsymbol{R}}_T\|_{0,T}^2. \tag{3.11}
$$

For $F \in \mathcal{F}_{\mathcal{T}}(\Omega)$, we make use of the face bubble function $b_F$ (see Ref. 40), which vanishes on $\partial\omega_F$, to construct $\boldsymbol{v}_F := \overline{J}_{F,1}b_F \in \boldsymbol{H}_0^1(\omega_F)$. By similar arguments, we derive

$$
\begin{aligned}
C\|\overline{\boldsymbol{J}}_{F,1}\|_{0,F}^2 &\le (\overline{\boldsymbol{J}}_{F,1}, \boldsymbol{v}_F)_F = (\boldsymbol{J}_{F,1}, \boldsymbol{v}_F)_F + (\overline{\boldsymbol{J}}_{F,1} - \boldsymbol{J}_{F,1}, \boldsymbol{v}_F)_F \\
&= (\boldsymbol{R}_T, \boldsymbol{v}_F)_{\omega_F} - (\nu(\cdot,|\boldsymbol{\nabla}\times\boldsymbol{u}|)\boldsymbol{\nabla}\times\boldsymbol{u} - \nu(\cdot,|\boldsymbol{\nabla}\times\boldsymbol{u}_{\mathcal{T}}|)\boldsymbol{\nabla}\times\boldsymbol{u}_{\mathcal{T}}, \boldsymbol{\nabla} \\
&\quad \times \boldsymbol{v}_F)_{\omega_F} + (\overline{\boldsymbol{J}}_{F,1} - \boldsymbol{J}_{F,1}, \boldsymbol{v}_F)_F.
\end{aligned}
$$

Then estimates $\|\boldsymbol{\nabla}\times\boldsymbol{v}_F\|_{0,\omega_F} \le Ch_F^{-1}\|\boldsymbol{v}_F\|_{0,\omega_F} \le Ch_F^{-1/2}\|\overline{\boldsymbol{J}}_F\|_{0,F}$, (3.11) and the triangle inequality imply that

$$
\begin{aligned}
Ch_F\|\boldsymbol{J}_{F,1}\|_{0,F}^2 \le \sum_{T\in\omega_F} &\Big(\|\boldsymbol{u}-\boldsymbol{u}_{\mathcal{T}}\|_{\boldsymbol{H}(\mathbf{curl};T)}^2 + h_T^2\|\boldsymbol{R}_T - \overline{\boldsymbol{R}}_T\|_{0,T}^2\Big) \\
&+ h_F\|\boldsymbol{J}_{F,1} - \overline{\boldsymbol{J}}_{F,1}\|_{0,F}^2.
\end{aligned} \tag{3.12}
$$

For the error indicator $h_T\|g\|_{0,T}$, taking $q = q_T = \overline{g}_T b_T \in H_0^1(T)$ in the second equation of (2.1) and arguing as above, we obtain

$$
Ch_T^2\|g\|_{0,T}^2 \le \|\boldsymbol{u}-\boldsymbol{u}_{\mathcal{T}}\|_{0,T}^2 + h_T^2\|g-\overline{g}_T\|_{0,T}^2. \tag{3.13}
$$

Let $\mathrm{E}_F(J_{F,2})$ be a constant extension of $J_{F,2}$ along the normal $\boldsymbol{n}_F$ or $-\boldsymbol{n}_F$ to $F$. Then using the second equation of (2.1) with $q = q_F = \mathrm{E}_F(J_{F,2})b_F \in H_0^1(\omega_F)$, the estimates $\|\boldsymbol{\nabla}q_F\|_{0,\omega_F} \le Ch_F^{-1}\|q_F\|_{0,\omega_F} \le Ch_F^{-1/2}\|J_{F,2}\|_{0,F}$, (3.13) and similar arguments, we obtain

$$
\begin{aligned}
C\|J_{F,2}\|_{0,F}^2 &\le (J_{F,2}, q_F)_F = (\boldsymbol{u}_{\mathcal{T}} - \boldsymbol{u}, \boldsymbol{\nabla}q_F)_{\omega_F} - (g, q_F)_{\omega_F} \\
&\le C(h_F^{-1/2}\sum_{T\in\omega_F}\|\boldsymbol{u}-\boldsymbol{u}_{\mathcal{T}}\|_{0,T} + h_F^{1/2}\sum_{T\in\omega_F}\|g\|_{0,T})\|J_{F,2}\|_{0,F}.
\end{aligned}
$$

Hence,

$$
Ch_F\|J_{F,2}\|_{0,F}^2 \le \sum_{T\in\omega_F}(\ \|\boldsymbol{u}-\boldsymbol{u}_{\mathcal{T}}\|_{0,T}^2 + h_T^2\|g-\overline{g}_T\|_{0,T}^2). \tag{3.14}
$$

Now we can see that the desired estimate (3.10) follows from (3.11) to (3.14). □

## 4. Adaptive Algorithm

On the basis of the reliable and efficient *a posteriori* error estimator (3.1)–(3.3), we now propose an adaptive algorithm for solving the quasilinear saddle point magnetostatic Maxwell system (1.1). In what follows, all dependences on triangulations are indicated by the number of refinements $k$.

**Algorithm 4.1.**

(1) (INITIALIZATION) Set $k := 0$ and choose an initial conforming mesh $\mathcal{T}_k$ such that $\nu$ is piecewise $W^{1,\infty}$ in its first variable.
(2) (SOLVE) Solve the discrete problem (2.12) on $\mathcal{T}_k$ for $\boldsymbol{u}_k \in \boldsymbol{V}_k$.
(3) (ESTIMATE) Compute the error estimator $\eta_k(\boldsymbol{u}_k, \boldsymbol{f}, g)$ defined in (3.1)–(3.3).
(4) (MARK) Mark a subset $\mathcal{M}_k \subseteq \mathcal{T}_k$ containing at least one element $\widetilde{T} \in \mathcal{T}_k$ with the largest local error indicator, i.e.

$$\eta_k(\boldsymbol{u}_k, \boldsymbol{f}, g, \widetilde{T}) = \max_{T \in \mathcal{T}_k} \eta_k(\boldsymbol{u}_k, \boldsymbol{f}, g, T). \tag{4.1}$$

(5) (REFINE) Refine each $T \in \mathcal{M}_k$ by bisection to get $\mathcal{T}_{k+1}$.
(6) Set $k := k + 1$ and go to Step (2).

It should be pointed out that several practical marking strategies, including the maximum strategy (see Ref. 2), the equidistribution strategy (see Ref. 21), the modified equidistribution strategy and Dörfler's strategy[19] satisfy the requirement (4.1). Let us close this section by proving the following stability result for the error estimator.

**Lemma 4.1.** *Let* $\{\boldsymbol{u}_k\}_{k=0}^{\infty}$ *be the sequence of discrete solutions by Algorithm* 4.1. *Then there holds*

$$\begin{aligned}\eta_k(\boldsymbol{u}_k, \boldsymbol{f}, g, T) \le C(&\|\boldsymbol{\nabla} \times \boldsymbol{u}_k\|_{0,\omega_T} + \|\boldsymbol{u}_k\|_{0,\omega_T} \\ &+ h_T\|\boldsymbol{f}\|_{0,T} + h_T\|g\|_{0,T}) \quad \forall T \in \mathcal{T}_k.\end{aligned} \tag{4.2}$$

**Proof.** An elementary calculation, together with $\boldsymbol{\nabla} \times \boldsymbol{\nabla} \times \boldsymbol{u}_k = \boldsymbol{0}$ on each $T \in \mathcal{T}_k$, shows that

$$\boldsymbol{f} - \boldsymbol{\nabla} \times (\nu(\boldsymbol{x}, |\boldsymbol{\nabla} \times \boldsymbol{u}_k|)\boldsymbol{\nabla} \times \boldsymbol{u}_k) = \boldsymbol{f} - \boldsymbol{\nabla}\nu(\boldsymbol{x}, |\boldsymbol{\nabla} \times \boldsymbol{u}_k|) \times (\boldsymbol{\nabla} \times \boldsymbol{u}_k).$$

As $\nu(\cdot, |\nabla \times \boldsymbol{u}_k|)$ is piecewise $W^{1,\infty}$ over $\mathcal{T}_0$, we have

$$h_T\|\boldsymbol{R}_T\|_{0,T} \le h_T\|\boldsymbol{f}\|_{0,T} + Ch_T\|\boldsymbol{\nabla} \times \boldsymbol{u}_k\|_{0,T}. \tag{4.3}$$

For two jump terms across $F \in \mathcal{F}_k(\Omega)$ shared by $T$, $T' \in \mathcal{T}_k$, the scaled trace theorem, the inverse estimate and the assumption (2.3) tell that

$$\begin{aligned}h_F^{1/2}\|\boldsymbol{J}_{F,1}\|_{0,F} &\le h_F^{1/2}(\|(\nu\boldsymbol{\nabla} \times \boldsymbol{u}_k)|_T\|_{0,F} + \|(\nu\boldsymbol{\nabla} \times \boldsymbol{u}_k)|_{T'}\|_{0,F}) \\ &\le C\|\boldsymbol{\nabla} \times \boldsymbol{u}_k\|_{0,\omega_F},\end{aligned} \tag{4.4}$$

$$h_F^{1/2}\|J_{F,2}\|_{0,F} \le C\|\boldsymbol{u}_k\|_{0,\omega_F}. \tag{4.5}$$

Then collecting (4.3)–(4.5) gives the desired estimate. □

## 5. Convergence

This section is devoted to the convergence analysis of the adaptive Algorithm 4.1. Our goal is to prove the strong $\boldsymbol{H}(\mathbf{curl})$-convergence of the sequence of discrete solutions $\{\boldsymbol{u}_k\}_{k=0}^{\infty}$ generated by Algorithm 4.1 towards the exact solution of the problem (2.1). Due to the special saddle-point nature of the current nonlinear Maxwell system, we need to develop a very different argument from those for the nonlinear elliptic problems in Refs. 22 and 39 in order to establish our desired strong $\boldsymbol{H}(\mathbf{curl})$-convergence. We start with a key limiting problem posed over the following spaces:

$$\boldsymbol{V}_\infty := \overline{\bigcup_{k\geq 0} \boldsymbol{V}_k} \quad (\text{in } \boldsymbol{H}(\mathbf{curl})\text{-norm}), \quad S_\infty := \overline{\bigcup_{k\geq 0} S_k} \ (\text{in } H^1\text{-norm}),$$

$$\boldsymbol{X}_\infty := \{\boldsymbol{v} \in \boldsymbol{V}_\infty \,|\, (\boldsymbol{v}, \boldsymbol{\nabla} q) = 0 \ \forall\, q \in S_\infty\},$$

where $\{\boldsymbol{V}_k\}_{k=0}^{\infty}$ and $\{S_k\}_{k=0}^{\infty}$ are generated by Algorithm 4.1. The general idea of using limiting spaces was used to analyze the convergence of an adaptive FEM in Ref. 5 for an one-dimensional boundary value problem, and was then generalized in Ref. 31 for linear elliptic problems. This general principle has been widely used in the analysis of adaptive FEMs, but its realization is often very different with a different problem. We can easily see from (2.11) and the definitions of $\boldsymbol{V}_\infty$ and $S_\infty$ that

$$\boldsymbol{\nabla} S_\infty \subset \boldsymbol{V}_\infty, \qquad \sup_{\mathbf{0}\neq \boldsymbol{v}\in \boldsymbol{V}_\infty} \frac{(\boldsymbol{v}, \boldsymbol{\nabla} q)}{\|\boldsymbol{v}\|_{\boldsymbol{H}(\mathbf{curl})}} \geq \|\boldsymbol{\nabla} q\|_0 \quad \forall\, q \in S_\infty. \tag{5.1}$$

In addition, though we know $\boldsymbol{X}_\infty$ is generally not a subspace $\boldsymbol{X}$, we demonstrated that an important Poincaré-type inequality is still true on $\boldsymbol{X}_\infty$ (see Lemma 5.1 in Ref. 41)

$$\|\boldsymbol{v}\|_0 \leq C \|\boldsymbol{\nabla} \times \boldsymbol{v}\|_0 \quad \forall\, \boldsymbol{v} \in \boldsymbol{X}_\infty \tag{5.2}$$

with the constant $C$ only depending on $\Omega$ and the shape-regularity of $\mathcal{T}_0$.

We can now study the following key limiting problem: Find $(\boldsymbol{u}_\infty, p_\infty) \in \boldsymbol{V}_\infty \times S_\infty$ such that

$$\begin{cases} (\nu(\boldsymbol{x}, |\boldsymbol{\nabla} \times \boldsymbol{u}_\infty|)\boldsymbol{\nabla} \times \boldsymbol{u}_\infty, \boldsymbol{\nabla} \times \boldsymbol{v}_\infty) + (\boldsymbol{v}_\infty, \boldsymbol{\nabla} p_\infty) = (\boldsymbol{f}, \boldsymbol{v}_\infty) & \forall\, \boldsymbol{v}_\infty \in \boldsymbol{V}_\infty, \\ (\boldsymbol{u}_\infty, \boldsymbol{\nabla} q_\infty) = -(g, q_\infty) & \forall\, q_\infty \in S_\infty. \end{cases} \tag{5.3}$$

The same as for the system (2.1), we know the problem (5.3) admits a unique solution thanks to (2.7), (2.6), (5.2) and (5.1), and $p_\infty \equiv 0$. We first show the following optimal estimate.

**Theorem 5.1.** *Let $\boldsymbol{u}_\infty$ be the solution of* (5.3) *and $\{\boldsymbol{u}_k\}_{k=0}^{\infty}$ be the sequence of discrete solutions generated by Algorithm* 4.1. *Then*

$$\|\boldsymbol{u}_\infty - \boldsymbol{u}_k\|_{\boldsymbol{H}(\mathbf{curl})} \leq C \inf_{\boldsymbol{v}_k \in \boldsymbol{V}_k} \|\boldsymbol{u}_\infty - \boldsymbol{v}_k\|_{\boldsymbol{H}(\mathbf{curl})} \to 0 \ \textit{as}\ k \to \infty. \tag{5.4}$$

**Proof.** Let $k \in \mathbb{N} \cup \{0\}$, and we introduce the set

$$\boldsymbol{X}_k(g) := \{\boldsymbol{v}_k \in \boldsymbol{V}_k \mid (\boldsymbol{v}_k, \boldsymbol{\nabla} q_k) = -(g, \boldsymbol{\nabla} q_k) \quad \forall\, q_k \in S_k\}$$

and $\boldsymbol{X}_k := \boldsymbol{X}_k(0)$. We point out that $\boldsymbol{X}_k(g) \neq \emptyset$ since $\boldsymbol{u}_k \in \boldsymbol{X}_k(g)$.

Since $\boldsymbol{u}_k - \boldsymbol{w}_k \in \boldsymbol{X}_k$ for every $\boldsymbol{w}_k \in \boldsymbol{X}_k(g)$, we deduce from (2.6), (2.7), (2.12), (2.13), (5.3), and $p_\infty = p_k = 0$ that there exists a constant $\widehat{C}_M > 0$, depending only on $\nu_1$, $\Omega$ and the shape-regularity of $\mathcal{T}_0$, such that

$$\begin{aligned}
\widehat{C}_M \|\boldsymbol{u}_k - \boldsymbol{w}_k\|^2_{\boldsymbol{H}(\mathbf{curl})} &\le \langle A\boldsymbol{u}_k - A\boldsymbol{w}_k, \boldsymbol{u}_k - \boldsymbol{w}_k\rangle \\
&= \langle A\boldsymbol{u}_k - A\boldsymbol{u}_\infty, \boldsymbol{u}_k - \boldsymbol{w}_k\rangle + \langle A\boldsymbol{u}_\infty - A\boldsymbol{w}_k, \boldsymbol{u}_k - \boldsymbol{w}_k\rangle \\
&= \langle A\boldsymbol{u}_\infty - A\boldsymbol{w}_k, \boldsymbol{u}_k - \boldsymbol{w}_k\rangle \\
&\le L\|\boldsymbol{u}_\infty - \boldsymbol{w}_k\|_{\boldsymbol{H}(\mathbf{curl})}\|\boldsymbol{u}_k - \boldsymbol{w}_k\|_{\boldsymbol{H}(\mathbf{curl})} \quad \forall\, \boldsymbol{w}_k \in \boldsymbol{X}_k(g),
\end{aligned}$$

which, together with the triangle inequality, gives

$$\|\boldsymbol{u}_\infty - \boldsymbol{u}_k\|_{\boldsymbol{H}(\mathbf{curl})} \le \left(1 + \frac{L}{\widehat{C}_M}\right) \inf_{\boldsymbol{w}_k \in \boldsymbol{X}_k(g)} \|\boldsymbol{u}_\infty - \boldsymbol{w}_k\|_{\boldsymbol{H}(\mathbf{curl})}. \tag{5.5}$$

For every $\boldsymbol{v}_k \in \boldsymbol{V}_k$, there exists a unique $\phi_k \in S_k$ such that

$$(\boldsymbol{\nabla}\phi_k, \boldsymbol{\nabla} q_k) = (\boldsymbol{u}_\infty - \boldsymbol{v}_k, \boldsymbol{\nabla} q_k) \quad \forall\, q_k \in S_k.$$

This solution satisfies

$$\|\boldsymbol{\nabla}\phi_k\|_0 \le \|\boldsymbol{u}_\infty - \boldsymbol{v}_k\|_{\boldsymbol{H}(\mathbf{curl})}. \tag{5.6}$$

Now, since $(\boldsymbol{\nabla}\phi_k + \boldsymbol{v}_k, \boldsymbol{\nabla} q_k) = (\boldsymbol{u}_\infty, \boldsymbol{\nabla} q_k) = -(g, q_k)$ holds for all $q_k \in S_k$, it follows that

$$\boldsymbol{\nabla}\phi_k + \boldsymbol{v}_k \in \boldsymbol{X}_k(g),$$

therefore we may set $\boldsymbol{w}_k = \boldsymbol{\nabla}\phi_k + \boldsymbol{v}_k$ in the right-hand side of (5.5) and use (5.6) to obtain that

$$\begin{aligned}
\|\boldsymbol{u}_\infty - \boldsymbol{u}_k\|_{\boldsymbol{H}(\mathbf{curl})} &\le \left(1 + \frac{L}{\widehat{C}_M}\right)\left(\|\boldsymbol{u}_\infty - \boldsymbol{v}_k\|_{\boldsymbol{H}(\mathbf{curl})} + \|\boldsymbol{\nabla}\phi\|_{\boldsymbol{H}(\mathbf{curl})}\right) \\
&\le 2\left(1 + \frac{L}{\widehat{C}_M}\right)\|\boldsymbol{u}_\infty - \boldsymbol{v}_k\|_{\boldsymbol{H}(\mathbf{curl})} \quad \forall\, \boldsymbol{v}_k \in \boldsymbol{V}_k.
\end{aligned}$$

In view of the density of $\bigcup_{k\ge 0} \boldsymbol{V}_k$ in $\boldsymbol{V}_\infty$, this inequality leads to the desired result. □

By virtue of Theorem 5.1, it suffices to prove that $\boldsymbol{u}_\infty$ is exactly the solution of (2.1) so that the convergence of $\{\boldsymbol{u}_k\}_{k=0}^\infty$ given by Algorithm 4.1 follows. In doing so, we split each $\mathcal{T}_k$ by Algorithm 4.1 as follows:

$$\mathcal{T}_k^+ := \bigcap_{l\ge k} \mathcal{T}_l, \quad \mathcal{T}_k^0 := \mathcal{T}_k \setminus \mathcal{T}_k^+, \quad \Omega_k^+ := \bigcup_{T\in\mathcal{T}_k^+} D_T, \quad \Omega_k^0 := \bigcup_{T\in\mathcal{T}_k^0} D_T.$$

That is, $\mathcal{T}_k^+$ consists of all elements not refined after the $k$th iteration while all elements in $\mathcal{T}_k^0$ are refined at least once after the $k$th iteration. It is easy to see

$\mathcal{T}_l^+ \subset \mathcal{T}_k^+$ for $l < k$ and $\mathcal{M}_k \subset \mathcal{T}_k^0$. We also define a mesh-size function $h_k : \overline{\Omega} \to \mathbb{R}^+$ almost everywhere by $h_k(\boldsymbol{x}) = h_T$ for $\boldsymbol{x}$ in the interior of an element $T \in \mathcal{T}_k$ and $h_k(\boldsymbol{x}) = h_F$ for $\boldsymbol{x}$ in the relative interior of a face $F \in \mathcal{F}_k$. Letting $\chi_k^0$ be the characteristic function of $\Omega_k^0$, then the mesh-size function $h_k(\boldsymbol{x})$ has the property (see Refs. 31 and 37)

$$\lim_{k\to\infty} \|h_k \chi_k^0\|_{L^\infty(\Omega)} = 0. \tag{5.7}$$

With the above preparations, we are now able to establish that the maximal error indicator among all the marked elements at each adaptive loop converges to zero.

**Lemma 5.1.** *Let $\{\mathcal{T}_k, \boldsymbol{V}_k, \boldsymbol{u}_k\}_{k=0}^\infty$ be the sequence of meshes, finite element spaces and discrete solutions generated by Algorithm* 4.1 *and $\mathcal{M}_k$ be the set of marked elements over $\mathcal{T}_k$. Then*

$$\lim_{k\to\infty} \max_{T\in\mathcal{M}_k} \eta_k(\boldsymbol{u}_k, \boldsymbol{f}, g, T) = 0. \tag{5.8}$$

**Proof.** We denote by $\widetilde{T}_k$ the element with the largest error indicator among $\mathcal{M}_k$. As $\widetilde{T}_k \in \mathcal{T}_k^0$, the local quasi-uniformity and (5.7) imply that

$$|\omega_{\widetilde{T}_k}| \le C|\widetilde{T}_k| \le C\|h_k \chi_k^0\|_{L^\infty(\Omega)}^3 \to 0. \tag{5.9}$$

By the stability estimate (4.2) and the triangle inequality,

$$\begin{aligned}
\eta_k(\boldsymbol{u}_k, \boldsymbol{f}, g, \widetilde{T}_k) &\le C(\|\boldsymbol{\nabla}\times\boldsymbol{u}_k\|_{0,\omega_{\widetilde{T}_k}} + \|\boldsymbol{u}_k\|_{0,\omega_{\widetilde{T}_k}} + \|\boldsymbol{f}\|_{0,\widetilde{T}_k} + \|g\|_{0,\widetilde{T}_k}) \\
&\le C(\|\boldsymbol{\nabla}\times\boldsymbol{u}_\infty\|_{0,\omega_{\widetilde{T}_k}} + \|\boldsymbol{\nabla}\times(\boldsymbol{u}_k - \boldsymbol{u}_\infty)\|_0 + \|\boldsymbol{u}_\infty\|_{0,\omega_{\widetilde{T}_k}} \\
&\quad + \|\boldsymbol{u}_k - \boldsymbol{u}_\infty\|_0 + \|\boldsymbol{f}\|_{0,\widetilde{T}_k} + \|g\|_{0,\widetilde{T}_k}).
\end{aligned}$$

Now the second and the fourth terms in the right-hand side go to zero by Theorem 5.1. The rest also go to zero due to (5.9) and the absolute continuity of $\|\cdot\|_0$ with respect to the Lebesgue measure. □

For every $k \in \mathbb{N}\cup\{0\}$, we introduce two linear bounded functionals $\mathcal{R}_1(\boldsymbol{u}_k) : \boldsymbol{H}_0(\mathbf{curl}) \to \mathbb{R}$ and $\mathcal{R}_2(\boldsymbol{u}_k) : H_0^1(\Omega) \to \mathbb{R}$ by

$$\langle \mathcal{R}_1(\boldsymbol{u}_k), \boldsymbol{v}\rangle := (\nu(\boldsymbol{x}, |\boldsymbol{\nabla}\times\boldsymbol{u}_k|)\boldsymbol{\nabla}\times\boldsymbol{u}_k, \boldsymbol{\nabla}\times\boldsymbol{v}) - (\boldsymbol{f}, \boldsymbol{v}) \quad \forall\, \boldsymbol{v} \in \boldsymbol{H}_0(\mathbf{curl}), \tag{5.10}$$

$$\langle \mathcal{R}_2(\boldsymbol{u}_k), q\rangle := (\boldsymbol{u}_k, \boldsymbol{\nabla} q) + (g, q) \quad \forall\, q \in H_0^1(\Omega). \tag{5.11}$$

Thanks to Theorem 5.1 and (2.3), the sequences $\{\|\mathcal{R}_1(\boldsymbol{u}_k)\|_{\boldsymbol{H}_0(\mathbf{curl})^*}\}_{k=0}^\infty$ and $\{\|\mathcal{R}_2(\boldsymbol{u}_k)\|_{H^{-1}(\Omega)}\}_{k=0}^\infty$ are bounded. Furthermore, since $p_k = 0$ holds for every $k \in \mathbb{N}\cup\{0\}$, it follows from (2.12) that

$$\langle \mathcal{R}_1(\boldsymbol{u}_k), \boldsymbol{v}\rangle = 0 \quad \forall\, \boldsymbol{v} \in \boldsymbol{V}_k, \quad \langle \mathcal{R}_2(\boldsymbol{u}_k), q\rangle = 0 \quad \forall\, q \in S_k \tag{5.12}$$

for every $k \in \mathbb{N}\cup\{0\}$.

**Lemma 5.2.** *The sequence of discrete solutions* $\{\boldsymbol{u}_k\}_{k=0}^{\infty}$ *generated by Algorithm* 4.1 *satisfies*

$$\lim_{k\to\infty}\langle\mathcal{R}_1(\boldsymbol{u}_k),\boldsymbol{v}\rangle=0\quad\forall\,\boldsymbol{v}\in\boldsymbol{H}_0(\mathbf{curl}),\tag{5.13a}$$

$$\lim_{k\to\infty}\langle\mathcal{R}_2(\boldsymbol{u}_k),q\rangle=0\quad\forall\,q\in H_0^1(\Omega).\tag{5.13b}$$

**Proof.** We first prove (5.13b). To this aim, for every $k\in\mathbb{N}\cup\{0\}$, we denote, respectively, by $I_k$ and $I_k^{sz}$ the standard nodal interpolation operator (see Ref. 12) and the Scott–Zhang quasi-interpolation operator[36] associated with $S_k$. Let $q\in C_0^\infty(\Omega)$, $l\in\mathbb{N}\cup\{0\}$, and $k\in\mathbb{N}$ with $k>l$. By virtue of (5.12), we deduce that

$$\begin{aligned}|\langle\mathcal{R}_2(\boldsymbol{u}_k),q\rangle|&=|(\boldsymbol{u}_k,\boldsymbol{\nabla}(q-I_kq))+(g,q-I_kq)|\\&=|(\boldsymbol{u}_k,\boldsymbol{\nabla}(q-I_kq-I_k^{sz}(q-I_kq)))+(g,q-I_kq-I_k^{sz}(q-I_kq))|\\&\le C\sum_{T\in\mathcal{T}_k}\eta_{k,2}(\boldsymbol{u}_k,g,T)\|q-I_kq\|_{1,D_T}\\&\le C(\eta_{k,2}(\boldsymbol{u}_k,g,\mathcal{T}_k\backslash\mathcal{T}_l^+)\|q-I_kq\|_{1,\Omega_l^0}+\eta_{k,2}(\boldsymbol{u}_k,g,\mathcal{T}_l^+)\|q-I_kq\|_{1,\Omega_l^+}),\end{aligned}$$

with a constant $C>0$, independent of $q$, $l$ and $k$. We note that the first inequality above follows from the error estimates of $I_k^{sz}$ (cf. (3.4)) and the elementwise integration by parts. Using the stability estimate (4.2), Theorem 5.1 and the error estimate for $I_k$ (see Ref. 12), we further derive

$$|\langle\mathcal{R}_2(\boldsymbol{u}_k),q\rangle|\le C_1\|h_l\|_{L^\infty(\Omega_l^0)}\|q\|_2+C_2\eta_{k,2}(\boldsymbol{u}_k,g,\mathcal{T}_l^+)\|q\|_2,\tag{5.14}$$

with two positive constants $C_1$ and $C_2$ independent of $q$, $l$, and $k$. Now, let $\epsilon>0$. In view of (5.7), there exists an index $l_\epsilon\in\mathbb{N}$ such that

$$C_1\|h_l\|_{L^\infty(\Omega_l^0)}\|q\|_2<\epsilon/2\quad\forall\,l\ge l_\epsilon.\tag{5.15}$$

On the other hand, since $\mathcal{T}_l^+\subset\mathcal{T}_k^+\subset\mathcal{T}_k$ for all $k>l$, the marking property (4.1) implies that

$$\eta_{k,2}(\boldsymbol{u}_k,g,\mathcal{T}_l^+)\le\sqrt{|\mathcal{T}_l^+|}\max_{T\in\mathcal{T}_l^+}\eta_{k,2}(\boldsymbol{u}_k,g,T)\le\sqrt{|\mathcal{T}_l^+|}\max_{T\in\mathcal{M}_k}\eta_k(\boldsymbol{u}_k,\boldsymbol{f},g,T).$$

Therefore, by virtue of Lemma 5.1, if necessary, we may increase the index $l_\epsilon\in\mathbb{N}$ such that

$$C_2\eta_{k,2}(\boldsymbol{u}_k,g,\mathcal{T}_l^+)\|q\|_2<\epsilon/2,\tag{5.16}$$

holds for all $k>l\ge l_\epsilon$. Concluding from (5.14)–(5.16) we have verified that for every positive real number $\epsilon>0$ there exists an index $l_\epsilon\in\mathbb{N}$ such that

$$|\langle\mathcal{R}_2(\boldsymbol{u}_k),q\rangle|<\epsilon\quad\forall\,q\in C_0^\infty(\Omega)\quad\forall\,k>l_\epsilon.$$

In conclusion, (5.13b) follows from this result along with the density of $C_0^\infty(\Omega)$ in $H_0^1(\Omega)$ and the boundedness of $\{\|\mathcal{R}_{2,k}(\boldsymbol{u}_k)\|_{H^{-1}(\Omega)}\}_{k=0}^{\infty}$.

We now prove (5.13a). To this aim, for a given $\boldsymbol{v} \in \boldsymbol{C}_0^\infty(\Omega)$, we set $\boldsymbol{w} := \boldsymbol{v} - \boldsymbol{\Pi}_k \boldsymbol{v} \in \boldsymbol{H}_0(\mathbf{curl}; \Omega)$, where $\boldsymbol{\Pi}_k$ is the curl-conforming Nédélec interpolant (cf. Ref. 27) associated with $\boldsymbol{V}_k$. Then, by virtue of (3.5), there exist $\boldsymbol{z} \in \boldsymbol{H}_0^1(\Omega)$ and $\varphi \in H_0^1(\Omega)$ such that $\boldsymbol{w} - \boldsymbol{\Pi}_k^s \boldsymbol{w} = \boldsymbol{z} + \boldsymbol{\nabla}\varphi$. Invoking (5.12), we deduce that

$$\langle \mathcal{R}_1(\boldsymbol{u}_k), \boldsymbol{v} \rangle = \langle \mathcal{R}_1(\boldsymbol{u}_k), \boldsymbol{v} - \boldsymbol{\Pi}_k \boldsymbol{v} \rangle = \langle \mathcal{R}_1(\boldsymbol{u}_k), \boldsymbol{w} - \boldsymbol{\Pi}_k^s \boldsymbol{w} \rangle = \langle \mathcal{R}_1(\boldsymbol{u}_k), \boldsymbol{z} + \boldsymbol{\nabla}\varphi \rangle. \tag{5.17}$$

As $\boldsymbol{\nabla} \cdot \boldsymbol{f} = 0$, we can easily find that

$$\langle \mathcal{R}_1(\boldsymbol{u}_k), \boldsymbol{\nabla}\varphi \rangle = 0. \tag{5.18}$$

Applying (5.18) to (5.17) and using an elementwise integration by parts, the trace theorem as well as the estimate (3.6), and recalling $\boldsymbol{w} = \boldsymbol{v} - \boldsymbol{\Pi}_k \boldsymbol{v}$, we further derive that

$$\begin{aligned}
\langle \mathcal{R}_1(\boldsymbol{u}_k), \boldsymbol{v} \rangle &= \langle \mathcal{R}_1(\boldsymbol{u}_k), \boldsymbol{z} \rangle \\
&= -\left( \sum_{T \in \mathcal{T}_k} (\boldsymbol{R}_T, \boldsymbol{z})_T - \sum_{F \in \mathcal{F}_k(\Omega)} (\boldsymbol{J}_{F,1}, \boldsymbol{z})_F \right) \\
&\le \sum_{T \in \mathcal{T}_k} h_T \|\boldsymbol{R}_T\|_{0,T} h_T^{-1} \|\boldsymbol{z}\|_{0,T} + \sum_{F \in \mathcal{F}_k(\Omega)} h_F^{1/2} \|\boldsymbol{J}_{F,1}\|_{0,F} h_F^{-1/2} \|\boldsymbol{z}\|_{0,F} \\
&\le C \sum_{T \in \mathcal{T}_k} (h_T^2 \|\boldsymbol{R}_T\|_{0,T}^2 + \sum_{F \subset \partial T \cap \Omega} h_F \|\boldsymbol{J}_{F,1}\|_{0,F}^2)^{1/2} (h_T^{-1} \|\boldsymbol{z}\|_{0,T} + |\boldsymbol{z}|_{1,T}) \\
&\le C \sum_{T \in \mathcal{T}_k} (h_T^2 \|\boldsymbol{R}_T\|_{0,T}^2 + \sum_{F \subset \partial T \cap \Omega} h_F \|\boldsymbol{J}_{F,1}\|_{0,F}^2)^{1/2} \|\boldsymbol{\nabla} \times (\boldsymbol{v} - \boldsymbol{\Pi}_k \boldsymbol{v})\|_{0,\widetilde{D}_T},
\end{aligned}$$

with a constant $C > 0$, independent of $k$ and $\boldsymbol{v}$. We now define a buffer layer of elements between $\mathcal{T}_l$ and $\mathcal{T}_k$ for $k, l \in \mathbb{N}$ with $k > l$

$$\mathcal{T}_{k,l}^b := \{T \in \mathcal{T}_k \backslash \mathcal{T}_l^+ \,|\, T \cap T' \neq \emptyset \ \forall\, T' \in \mathcal{T}_l^+\}.$$

We know from $\mathcal{T}_l^+ \subset \mathcal{T}_k^+ \subset \mathcal{T}_k$ and the uniform shape-regularity of $\{\mathcal{T}_k\}$ that

$$|\mathcal{T}_{k,l}^b| \le C |\mathcal{T}_l^+| \tag{5.19}$$

with constant $C$ depending only on the initial mesh $\mathcal{T}_0$, and $\widetilde{D}_T \subset \Omega_l^0$ for any $T \in \mathcal{T}_k \backslash (\mathcal{T}_l^+ \cup \mathcal{T}_{k,l}^b)$. Splitting $\mathcal{T}_k$ into $\mathcal{T}_l^+ \cup \mathcal{T}_{k,l}^b$ and $\mathcal{T}_k \setminus (\mathcal{T}_l^+ \cup \mathcal{T}_{k,l}^b)$ for $k > l$, and noting that $\bigcup_{T \in \mathcal{T}_k \backslash (\mathcal{T}_l^+ \cup \mathcal{T}_{k,l}^b)} \widetilde{D}_T \subseteq \Omega_l^0$, we can further proceed to derive

$$\begin{aligned}
|\langle \mathcal{R}_1(\boldsymbol{u}_k), \boldsymbol{v} \rangle| &\le C \sum_{T \in \mathcal{T}_k} \eta_{k,1}(\boldsymbol{u}_k, \boldsymbol{f}, T) \|\boldsymbol{\nabla} \times (\boldsymbol{v} - \boldsymbol{\Pi}_k \boldsymbol{v})\|_{0,\widetilde{D}_T} \\
&\le C(\eta_{k,1}(\boldsymbol{u}_k, \boldsymbol{f}, \mathcal{T}_k \backslash (\mathcal{T}_l^+ \cup \mathcal{T}_{k,l}^b)) \|\boldsymbol{\nabla} \times (\boldsymbol{v} - \boldsymbol{\Pi}_k \boldsymbol{v})\|_{0,\Omega_l^0} \\
&\quad + \eta_{k,1}(\boldsymbol{u}_k, \boldsymbol{f}, \mathcal{T}_l^+ \cup \mathcal{T}_{k,l}^b) \|\boldsymbol{\nabla} \times (\boldsymbol{v} - \boldsymbol{\Pi}_k \boldsymbol{v})\|_0),
\end{aligned}$$

which, along with the stability estimate (4.2) in Lemma 4.1, Theorem 5.1 and the interpolation error estimate for $\boldsymbol{\Pi}_k$ (see Ref. 15), implies

$$|\langle \mathcal{R}_1(\boldsymbol{u}_k), \boldsymbol{v}\rangle| \le C_3 \|h_l\|_{L^\infty(\Omega_l^0)} \|\boldsymbol{v}\|_2 + C_4 \eta_{k,1}(\boldsymbol{u}_k, \boldsymbol{f}, \mathcal{T}_l^+ \cup \mathcal{T}_{k,l}^b) \|\boldsymbol{v}\|_2. \quad (5.20)$$

As before, the property (5.7) allows the first term to be small enough for sufficiently large $l$. Using (4.1) and (5.19), we have

$$\begin{aligned}\eta_{k,1}(\boldsymbol{u}_k, \boldsymbol{f}, \mathcal{T}_l^+ \cup \mathcal{T}_b^{k,l}) &\le \sqrt{|\mathcal{T}_l^+| + |\mathcal{T}_b^{k,l}|} \max_{T \in \mathcal{T}_l^+ \cup \mathcal{T}_b^{k,l}} \eta_{k,1}(\boldsymbol{u}_k, \boldsymbol{f}, T) \\ &\le C\sqrt{|\mathcal{T}_l^+|} \max_{T \in \mathcal{M}_k} \eta_{k,1}(\boldsymbol{u}_k, \boldsymbol{f}, T).\end{aligned}$$

This and (5.8) indicate that the second term in the right-hand side of (5.20) is also small for all $k > l$ after fixing a sufficiently large $l$. It follows from (5.20) and these two facts that $\lim_{k\to\infty}\langle \mathcal{R}_1(\boldsymbol{u}_k), \boldsymbol{v}\rangle = 0$ for any $\boldsymbol{v} \in \boldsymbol{C}_0^\infty(\Omega)$. Then the density argument gives the first convergence. □

**Remark 5.1.** In the above proof, the key idea is a split of $\Omega$ into two parts: $\Omega_l^0$ and $\Omega_l^+$. Over the former we use local approximation properties of $I_k$, $\boldsymbol{\Pi}_k$ and (5.7) while the marking property (4.1) applies to the latter for $k > l$

$$\eta_k(\boldsymbol{u}_k, \boldsymbol{f}, g, \mathcal{T}_l^+) \le C\sqrt{|\mathcal{T}_l^+|} \max_{T \in \mathcal{M}_k} \eta_k(\boldsymbol{u}_k, \boldsymbol{f}, g, T).$$

From this and (5.8), we find that there holds for a fixed iteration $l$

$$\lim_{k\to\infty} \eta_k(\boldsymbol{u}_k, \boldsymbol{f}, g, \mathcal{T}_l^+) = 0.$$

Recalling that the Lagrange multiplier $p$ associated with (2.1) vanishes since the right-hand $\boldsymbol{f}$ is divergence-free, we can now conclude a crucial auxiliary result using the two lemmas above.

**Lemma 5.3.** *The solution* $\boldsymbol{u}_\infty \in \boldsymbol{H}_0(\mathbf{curl})$ *of* (5.3) *solves the original quasilinear Maxwell system*

$$\begin{cases} (\nu(\boldsymbol{x}, |\boldsymbol{\nabla} \times \boldsymbol{u}_\infty|)\boldsymbol{\nabla} \times \boldsymbol{u}_\infty, \boldsymbol{\nabla} \times \boldsymbol{v}) = (\boldsymbol{f}, \boldsymbol{v}) & \forall\, \boldsymbol{v} \in \boldsymbol{H}_0(\mathbf{curl}), \\ (\boldsymbol{u}_\infty, \boldsymbol{\nabla} q) = -(g, q) & \forall\, q \in H_0^1(\Omega). \end{cases} \quad (5.21)$$

**Proof.** We first prove the second variational equality in (5.21). For any $q \in H_0^1(\Omega)$, it follows from (5.11) that for every $k \in \mathbb{N}$,

$$(\boldsymbol{u}_\infty, \boldsymbol{\nabla} q) + (g, q) = (\boldsymbol{u}_\infty - \boldsymbol{u}_k, \boldsymbol{\nabla} q) + \langle \mathcal{R}_2(\boldsymbol{u}_k), q\rangle.$$

Then, taking the limit $k \to \infty$, we get from Theorem 5.1 and (5.13b) that

$$(\boldsymbol{u}_\infty, \boldsymbol{\nabla} q) + (g, q) = \lim_{k\to\infty} ((\boldsymbol{u}_\infty - \boldsymbol{u}_k, \boldsymbol{\nabla} q) + \langle \mathcal{R}_2(\boldsymbol{u}_k), q\rangle) = 0,$$

so the second variational equality of (5.21) is valid.

Next, let $\boldsymbol{v} \in \boldsymbol{H}_0(\mathbf{curl})$. In view of (5.10) and (5.3) along with $p_\infty \equiv 0$, it holds for every $k \in \mathbb{N}$ that

$$\begin{aligned} |(\nu(\boldsymbol{x}, |\boldsymbol{\nabla} \times \boldsymbol{u}_\infty|)\boldsymbol{\nabla} \times \boldsymbol{u}_\infty, \boldsymbol{\nabla} \times \boldsymbol{v}) - (\boldsymbol{f}, \boldsymbol{v})| &= |\langle A\boldsymbol{u}_\infty - A\boldsymbol{u}_k, \boldsymbol{v}\rangle + \langle \mathcal{R}_1(\boldsymbol{u}_k), \boldsymbol{v}\rangle| \\ &\underbrace{\leq}_{(2.7)} L\|\boldsymbol{u}_k - \boldsymbol{u}_\infty\|_{\boldsymbol{H}(\mathbf{curl})}\|\boldsymbol{v}\|_{\boldsymbol{H}(\mathbf{curl})} \\ &\quad + |\langle \mathcal{R}_1(\boldsymbol{u}_k), \boldsymbol{v}\rangle|. \end{aligned}$$

Then, taking the limit $k \to \infty$, it follows from Theorem 5.1 and (5.13a) that

$$(\nu(\boldsymbol{x}, |\boldsymbol{\nabla} \times \boldsymbol{u}_\infty|)\boldsymbol{\nabla} \times \boldsymbol{u}_\infty, \boldsymbol{\nabla} \times \boldsymbol{v}) = (\boldsymbol{f}, \boldsymbol{v}),$$

which completes the proof. □

Now the following strong convergence is a consequence of Lemma 5.3 and Theorem 5.1.

**Theorem 5.2.** *The sequence of discrete solutions* $\{\boldsymbol{u}_k\}_{k=0}^\infty$ *generated by Algorithm* 4.1 *converges strongly with respect to the* $\boldsymbol{H}(\mathbf{curl})$*-topology towards the solution* $\boldsymbol{u} \in \boldsymbol{H}_0(\mathbf{curl})$ *of* (2.1).

We end this section with the desired vanishing property of the estimators generated by our adaptive algorithm.

**Theorem 5.3.** *The sequence* $\{\eta_k(\boldsymbol{u}_k, \boldsymbol{f}, g)\}_{k=0}^\infty$ *of the estimators generated by Algorithm* 4.1 *converges to zero.*

**Proof.** We split the estimator as

$$\eta_k^2(\boldsymbol{u}_k, \boldsymbol{f}, g) = \eta_k^2(\boldsymbol{u}_k, \boldsymbol{f}, g, \mathcal{T}_l^+) + \eta_k^2(\boldsymbol{u}_k, \boldsymbol{f}, g, \mathcal{T}_k \backslash \mathcal{T}_l^+) \tag{5.22}$$

for $k > l$. The local lower bound (3.10) allows

$$\eta_k^2(\boldsymbol{u}_k, \boldsymbol{f}, g, \mathcal{T}_k \backslash \mathcal{T}_l^+) \leq C(\|\boldsymbol{u} - \boldsymbol{u}_k\|_{\boldsymbol{H}(\mathbf{curl})}^2 + \mathrm{osc}_k^2(\boldsymbol{f}, g, \mathcal{T}_k \backslash \mathcal{T}_l^+)).$$

Since $\overline{\boldsymbol{R}}_T$ is the best $L^2$-projection of $\boldsymbol{R}_T$ onto the constant space over $T$, $\boldsymbol{\nabla} \times \boldsymbol{\nabla} \times \boldsymbol{u}_k = \boldsymbol{0}$ and $\nu(\cdot, |\boldsymbol{\nabla} \times \boldsymbol{u}_k|)$ is $W^{1,\infty}$ in the first variable,

$$\begin{aligned} h_T\|\boldsymbol{R}_T - \overline{\boldsymbol{R}}_T\|_{0,T} &\leq h_T\|\boldsymbol{f} - \boldsymbol{\nabla}\nu(\boldsymbol{x}, |\boldsymbol{\nabla} \times \boldsymbol{u}_k|) \times (\boldsymbol{\nabla} \times \boldsymbol{u}_k)\|_{0,T} \\ &\leq h_T\|\boldsymbol{f}\|_{0,T} + \|\boldsymbol{\nabla}\nu\|_{L^\infty(T)}h_T\|\boldsymbol{\nabla} \times \boldsymbol{u}_k\|_{0,T} \\ &\leq Ch_T(\|\boldsymbol{f}\|_{0,T} + \|\boldsymbol{\nabla} \times \boldsymbol{u}_k\|_{0,T}). \end{aligned}$$

Likewise,

$$h_T\|g - \overline{g}_T\|_{0,T} \leq h_T\|g\|_{0,T}.$$

We denote by $\overline{[\cdot]}$ the average of $[\cdot]$ over $F$, by $\overline{\nu}_T(\cdot, |\boldsymbol{\nabla} \times \boldsymbol{u}_k|)$ the average of $\nu(\cdot, |\boldsymbol{\nabla} \times \boldsymbol{u}_k|)$ over $T \in \omega_F$. Then we apply the scaled trace theorem and the Poincaré

inequality and using the fact that $|\boldsymbol{\nabla}\times\boldsymbol{u}_k|$ is a piecewise constant over $\mathcal{T}_k$ to deduce that

$$\begin{aligned} h_F^{1/2}\|\boldsymbol{J}_{F,1}-\overline{\boldsymbol{J}}_{F,1}\|_{0,F} &\le h_F^{1/2}\sum_{T\in\omega_F}\|(\nu-\overline{\nu}_T)(\boldsymbol{\nabla}\times\boldsymbol{u}_k|_T)\times\boldsymbol{n}_F\|_{0,F} \\ &\le C\sum_{T\in\omega_F}(\|\nu-\overline{\nu}_T\|_{L^\infty(T)}+h_F\|\boldsymbol{\nabla}\nu\|_{L^\infty(T)})\|\boldsymbol{\nabla}\times\boldsymbol{u}_k\|_{0,T} \\ &\le C\sum_{T\in\omega_F}h_T\|\boldsymbol{\nabla}\times\boldsymbol{u}_k\|_{0,T}. \end{aligned}$$

Noting the uniform boundedness of $\|\boldsymbol{\nabla}\times\boldsymbol{u}_k\|_0$ in terms of $k$ from Theorem 5.2 and using the relation (5.22), we can arrive at

$$\eta_k^2(\boldsymbol{u}_k,\boldsymbol{f},g)\le C(\eta_k^2(\boldsymbol{u}_k,\boldsymbol{f},g,\mathcal{T}_l^+)+\|\boldsymbol{u}-\boldsymbol{u}_k\|^2_{\boldsymbol{H}(\mathbf{curl})}+\|h_l\|^2_{L^\infty(\Omega_l^0)}).$$

Now by (5.7), the third term in the right-hand side tends to zero as $l\to\infty$. Thanks to Remark 5.1 and Theorem 5.2 we may fix a large $l$ and choose a suitable $k>l$ such that the first term and the second term in the right-hand side are also sufficiently small. This leads to the conclusion. □

## 6. Numerical Experiments

Based on the underlying regularity assumption (Assumption 2.1), we construct an example for the nonlinear reluctivity function. Let us note that this example is merely academic and it is used to demonstrate the numerical performance of our adaptive algorithm more accurately as we know the exact solution analytically. We introduce the function

$$\nu:\mathbb{R}\to\mathbb{R}^+,\quad \nu(s)=1-\frac{1}{2(s^2+1)}. \tag{6.1}$$

Obviously, this function satisfies

$$\lim_{s\to\infty}\nu(s)=1\quad\text{and}\quad \frac{1}{2}\le\nu(s)\le 1\quad\forall\, s\in\mathbb{R}.$$

Furthermore, it is easy to verify that the function $\xi:\mathbb{R}\to\mathbb{R}$, $\xi(s):=\nu(s)s$, is continuously differentiable with $\xi'(s)=\dfrac{2s^4+5s^2+1}{2(s^2+1)^2}$. Then, straightforward computations yield that

$$\frac{1}{2}\le\xi'(s)\le\frac{34}{32}\quad\forall\, s\in\mathbb{R},$$

and consequently the mean value theorem implies for all $s,t\in\mathbb{R}$ that

$$(\xi(s)-\xi(t))(s-t)\ge\frac{1}{2}(s-t)^2\quad\text{and}\quad|\xi(s)-\xi(t)|\le\frac{34}{32}|s-t|.$$

Therefore, the reluctivity function (6.1) satisfies Assumption 2.1. We specify the computational domain $\Omega$ to be an L-shaped domain, defined by

$$\Omega:=(-1,1)\times(-1,1)\times(0,1)\backslash[0,1]\times[0,1]\times[0,1]. \tag{6.2}$$

In view of (6.2), the function

$$\vartheta : \Omega \to \mathbb{R}, \quad \vartheta(\boldsymbol{x}) = \sin(\pi x_1)\sin(\pi x_2)\sin(\pi x_3) \tag{6.3}$$

is of class $H_0^1(\Omega)$ such that $\nabla\vartheta \in \boldsymbol{H}_0(\mathbf{curl})$. For this reason, setting

$$\boldsymbol{f} \equiv 0 \quad \text{and} \quad g := \Delta\vartheta = -3\pi^2\vartheta,$$

the solution of (1.1) is then obtained by the gradient field $\boldsymbol{u} = \nabla\vartheta$. With this analytical solution, we shall test the numerical performance of our adaptive Algorithm 4.1. To this aim, we implemented Algorithm 4.1 in a Python script using the open source software FEniCS.[30] Here, the step SOLVE of Algorithm 4.1 was carried out using the Kačanov iteration:

(1) Set $n = 1$ and choose $\boldsymbol{u}_{\mathcal{T}_k}^{(0)} \in \boldsymbol{V}_{\mathcal{T}_k}$.
(2) Solve the linear system for $\boldsymbol{u}_{\mathcal{T}_k}^{(n)} \in \boldsymbol{V}_{\mathcal{T}_k}$:

$$\begin{cases} (\nu(|\boldsymbol{\nabla} \times \boldsymbol{u}_{\mathcal{T}_k}^{(n-1)}|)\boldsymbol{\nabla} \times \boldsymbol{u}_{\mathcal{T}_k}^{(n)}, \boldsymbol{\nabla} \times \boldsymbol{v}_{\mathcal{T}_k}) + (\boldsymbol{v}_{\mathcal{T}_k}, \boldsymbol{\nabla} p_{\mathcal{T}_k}^{(n)}) \\ \quad = (\boldsymbol{f}, \boldsymbol{v}_{\mathcal{T}_k}) & \forall\, \boldsymbol{v}_{\mathcal{T}_k} \in \boldsymbol{V}_{\mathcal{T}_k}, \\ (\boldsymbol{u}_{\mathcal{T}_k}^{(n)}, \boldsymbol{\nabla} q_{\mathcal{T}_k}) = -(g, q_{\mathcal{T}_k}) & \forall\, q_{\mathcal{T}_k} \in S_{\mathcal{T}_k}. \end{cases} \tag{6.4}$$

(3) If $\|\boldsymbol{u}_{\mathcal{T}_k}^{(n)} - \boldsymbol{u}_{\mathcal{T}_k}^{(n-1)}\|_{\boldsymbol{H}(\mathbf{curl})} < 10^{-8}$, STOP; otherwise set $n = n + 1$ and go to Step (2).

For our numerical experiments, we used zero initial data, and the linear system (6.4) was solved by the build-in preconditioned MinRes solver of FEniCS.

In the step MARK of Algorithm 4.1, elements of the simplicial triangulation $\mathcal{T}_k$ are marked for refinement based on the information provided by the proposed *a posteriori* error estimator $\eta_k(\boldsymbol{u}_k, \boldsymbol{f}, g) = \eta_{\mathcal{T}_k}(\boldsymbol{u}_k, \boldsymbol{f}, g, \mathcal{T}_k)$ (cf. (3.1)–(3.3) for its definition). Here, we employ Dörfler's strategy[19] with the associated bulk criterion $\theta = 0.6$. Thereafter, all marked elements are subdivided by the build-in bisection algorithm of FEniCS. Finally, we stop Algorithm 4.1 if the number of the degrees of freedom (DoF) in the finite element space $\boldsymbol{V}_{\mathcal{T}_k}$ exceeds a given maximum number $\mathrm{DoF}^*$, which is set to $\mathrm{DoF}^* = 4 \cdot 10^6$ for the first example and $\mathrm{DoF}^* = 1 \cdot 10^6$ for the second one.

In Fig. 1, we present the exact error $\|\boldsymbol{u} - \boldsymbol{u}_k\|_{\boldsymbol{H}(\mathbf{curl})}$ resulting from the uniform mesh refinement compared with the one based on the adaptive mesh refinement using the proposed error estimator $\eta_k(\boldsymbol{u}_k, \boldsymbol{f}, g)$. Observing Fig. 1, we may infer a better numerical performance of the adaptive method over the standard uniform mesh refinement. This can be more quantitatively clarified by evaluating the experimental rate of convergence (ERC) using two consecutive discrete solutions and DoF

$$\mathrm{ERC}_k = \left| \frac{\log(\|\boldsymbol{u} - \boldsymbol{u}_k\|_{\boldsymbol{H}(\mathbf{curl})}) - \log(\|\boldsymbol{u} - \boldsymbol{u}_{k-1}\|_{\boldsymbol{H}(\mathbf{curl})})}{\log(\mathrm{DoF}_k) - \log(\mathrm{DoF}_{k-1})} \right|.$$

The values of $\mathrm{ERC}_k$ for the uniform and adaptive refinement methods with various values for $\mathrm{DoF}_k$ are depicted in Tables 1 and 2, respectively. These results reconfirm

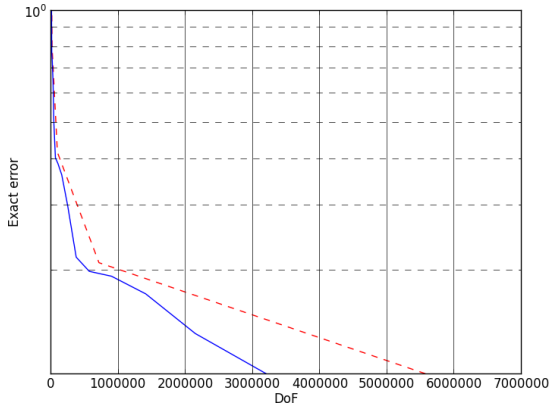


Fig. 1. Exact error for uniform (dash line) and adaptive mesh refinement (straight line).

Table 1. Experimental rate of convergence for the adaptive refinement method.

| $\mathrm{DoF}_k$ | 156093 | 244497 | 1405368 | 2143814 | 3204062 |
|---|---|---|---|---|---|
| $\|\boldsymbol{u}-\boldsymbol{u}_k\|_{\boldsymbol{H}(\mathbf{curl})}$ | 0.3624 | 0.2993 | 0.1735 | 0.1357 | 0.1057 |
| $\mathrm{ERC}_k$ | — | 0.4263 | 0.3118 | 0.5819 | 0.6218 |

Table 2. Experimental rate of convergence for the uniform refinement method.

| $\mathrm{DoF}_k$ | 1700 | 12136 | 91472 | 709792 | 5591360 |
|---|---|---|---|---|---|
| $\|\boldsymbol{u}-\boldsymbol{u}_k\|_{\boldsymbol{H}(\mathbf{curl})}$ | 1.3814 | 0.8007 | 0.4166 | 0.2104 | 0.1055 |
| $\mathrm{ERC}_k$ | — | 0.3780 | 0.3167 | 0.3428 | 0.3352 |

the better convergence of the adaptive algorithm over the standard uniform mesh refinement, but the improvement may not be seen so significant as the exact solution is smooth, without any singularities, which are the main targets of the adaptive method.

Furthermore, we show in Table 3 the exact error $\|\boldsymbol{u}-\boldsymbol{u}_k\|_{\boldsymbol{H}(\mathbf{curl})}$ and the estimator $\eta_k(\boldsymbol{u}_k, \boldsymbol{f}, g)$ at each adaptive discretization level. In particular, the numerical results illustrate our theoretical findings concerning the reliability of the proposed estimator (Theorem 3.1) and the convergence of Algorithm 4.1 (Theorem 5.2). In the last column of Table 3, we report the effectivity index

$$\mathrm{I}_k := \frac{\eta_k(\boldsymbol{u}_k, \boldsymbol{f}, g)}{\|\boldsymbol{u}-\boldsymbol{u}_k\|_{\boldsymbol{H}(\mathbf{curl})}}.$$

According to our numerical results, we find that $\mathrm{I}_k \approx 5$, which shows a reliable and accurate prediction of the exact energy error by our a posterior error estimator. Figure 2 displays the adaptive mesh after 15 refinement steps in Algorithm 4.1, over which the computed solution $\boldsymbol{u}_{15}$ is depicted in Fig. 3 (left). For comparison, the exact solution $\boldsymbol{u} = \nabla\vartheta$ is visualized in Fig. 3 (right).

Table 3. Convergence history and effectivity index.

| $k$ | DoF | $\|\boldsymbol{u}-\boldsymbol{u}_k\|_{\boldsymbol{H}(\mathbf{curl})}$ | $\eta_k(\boldsymbol{u}_k,\boldsymbol{f},g)$ | $\mathrm{I}_k$ |
|---|---|---|---|---|
| 0 | 1700 | 1.3814 | 7.7770 | 5.6299 |
| 1 | 2372 | 1.3213 | 7.3392 | 5.5543 |
| 2 | 3416 | 1.1753 | 6.4422 | 5.4813 |
| 3 | 5549 | 0.9272 | 5.2076 | 5.6162 |
| 4 | 8000 | 0.7692 | 4.4217 | 5.7482 |
| 5 | 15116 | 0.7298 | 3.7953 | 5.2003 |
| 6 | 26346 | 0.6503 | 3.2883 | 5.0562 |
| 7 | 39028 | 0.4994 | 2.7918 | 5.5901 |
| 8 | 61774 | 0.4026 | 2.2942 | 5.6982 |
| 9 | 98444 | 0.3890 | 2.0323 | 5.2251 |
| 10 | 156093 | 0.3624 | 1.7892 | 4.9378 |
| 11 | 244497 | 0.2993 | 1.5761 | 5.2669 |
| 12 | 371258 | 0.2177 | 1.2741 | 5.8539 |
| 13 | 566179 | 0.1994 | 1.1120 | 5.5763 |
| 14 | 896464 | 0.1935 | 0.9791 | 5.0590 |
| 15 | 1405368 | 0.1735 | 0.8738 | 5.0374 |
| 16 | 2143814 | 0.1357 | 0.7454 | 5.4914 |
| 17 | 3204062 | 0.1057 | 0.6184 | 5.8480 |

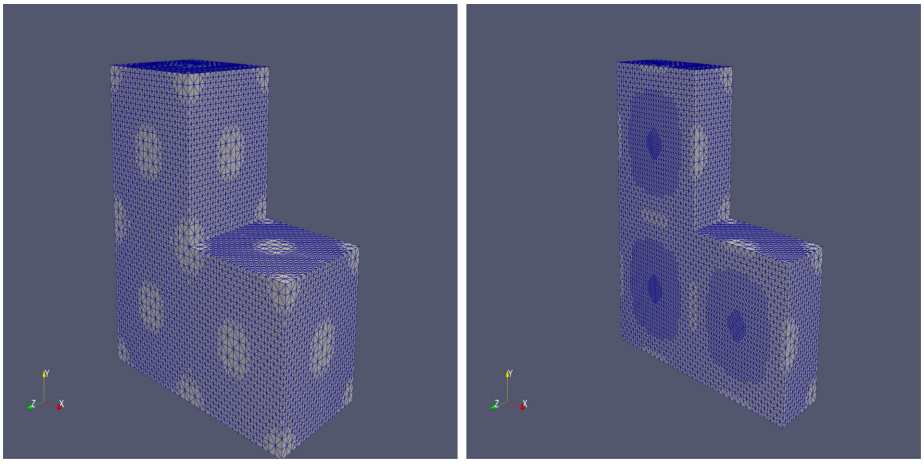

Fig. 2. Adaptive mesh and its cross section generated by Algorithm 4.1 for $k = 15$.

### 6.1. *A test with a jumping nonlinear coefficient and unknown solution*

We present now a test case involving jump discontinuities (with respect to the space variable) in the nonlinear magnetic reluctivity. More precisely, let us consider

$$\nu : \Omega \times \mathbb{R} \to \mathbb{R}^+, \quad \nu(\boldsymbol{x}, s) = 1 - \chi_{[0,1]}(x_1)\frac{1}{4(s^2+1)} - \chi_{[0,1]}(x_2)\frac{1}{4(s^2+1)}, \tag{6.5}$$

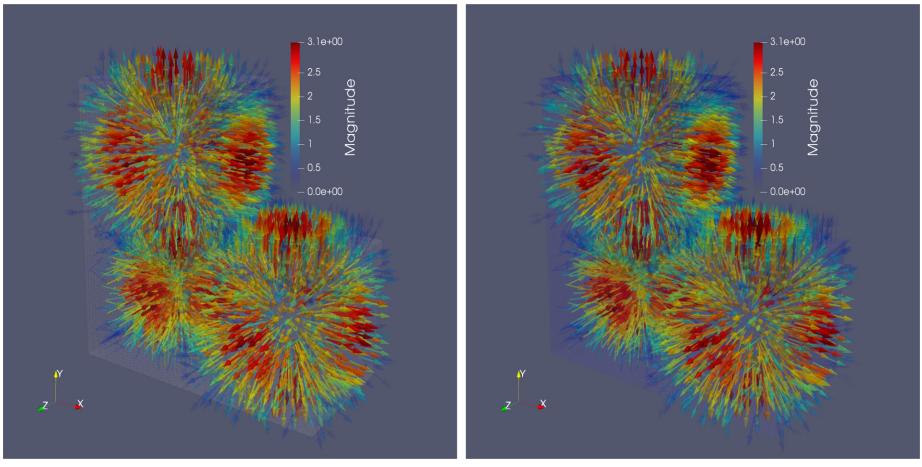


Fig. 3. Computed solution $\boldsymbol{u}_{15}$ on the adaptive mesh (left) and the exact solution $\boldsymbol{u}$ (right).

where $\chi_{[0,1]} : \mathbb{R} \to \mathbb{R}$ denotes the characteristic function of the interval $[0, 1]$. As in the first example, the reluctivity function (6.5) satisfies Assumption 2.1. Furthermore, we choose the data

$$g \equiv 0 \quad \text{and} \quad \boldsymbol{f} = (0, 0, 100\chi_\omega), \tag{6.6}$$

where $\chi_\omega$ denotes the characteristic function of the subset $\omega := \{\boldsymbol{x} \in \Omega \mid x_1^2 + x_2^2 < 10^{-3}\}$. We note that the function $\boldsymbol{f}$ is not continuous but divergence-free as its third component is independent of $x_3$. Differently from the previous example, the solution of (1.1) cannot be described analytically. Moreover, due to the non-convex structure of the computational domain, the jump discontinuities of the nonlinear permeability (6.5) and the non-smoothness of the given data (6.6), a smooth solution cannot be expected. In general, the solution enjoys only the regularity property $\boldsymbol{H}_0(\mathbf{curl}) \cap \boldsymbol{H}^s(\Omega)$ for some $s \in (0.5, 1)$ and may feature strong singularities (see Refs. 16 and 17). To deal with this issue, our adaptive edge element method may be useful for predicting the behavior of the unknown solution and capturing its local singularities. Figure 4 depicts the chosen initial mesh ($k = 0$) and the adaptive meshes generated by Algorithm 4.1 for different levels $k = 5, 10, 15$ with the bulk criterion $\theta = 0.3$ in Dörfler's strategy.[19] It is notable that a local refinement mainly occurs in the concave edge of $\Omega$. Due to the choice of $\boldsymbol{f}$, this behavior is not surprising. Next, in Fig. 5, we plot the computed solution $\boldsymbol{u}_{15}$ on the finest adaptive mesh (DoF $= 1.471919 \cdot 10^6$) generated by Algorithm 4.1. Indeed, we observe that the solution is mainly concentrated in the concave edge of $\Omega$ and vanishes outside this region.

Since the true solution for this example is unknown, we consider $\boldsymbol{u}_{ref} = \boldsymbol{u}_{15}$ as the reference solution to test the convergence behavior of the adaptive method, including the experimental rate of convergence ($\mathrm{ERC}_k$) and the associated efficiency index ($\mathrm{I}_k$). The numerical results are depicted in Table 4. Similar to the previous example, we observe a convergence behavior of both the error and the estimator

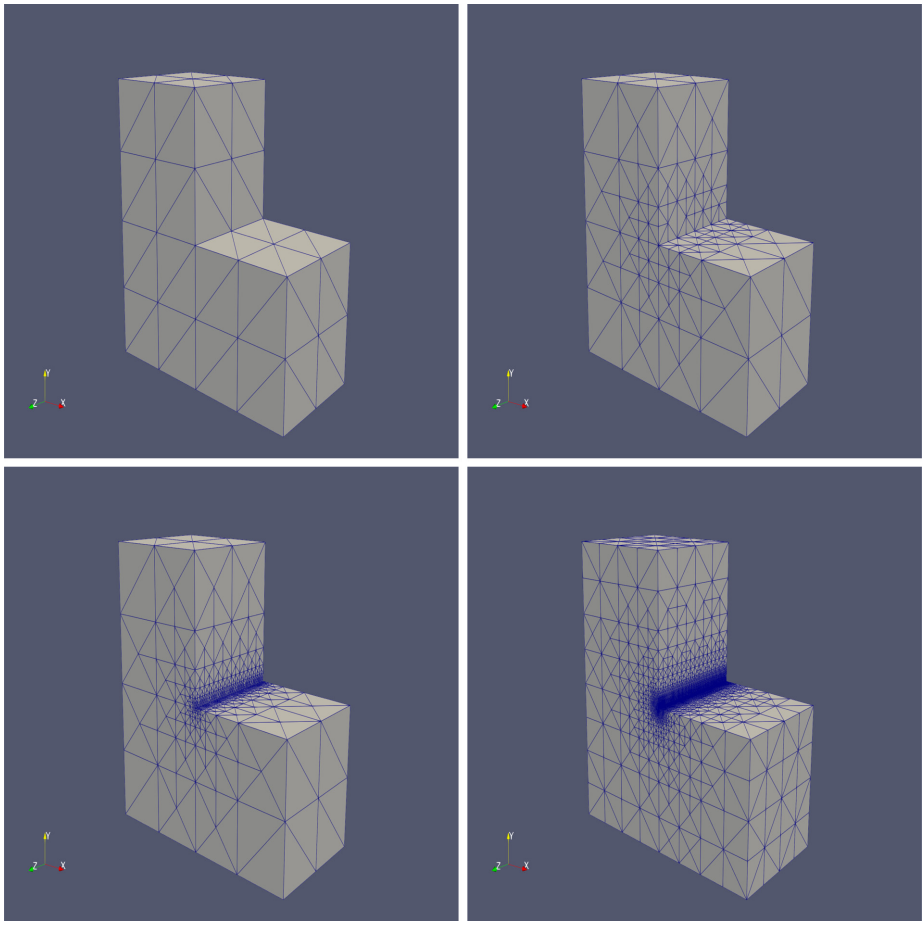

Fig. 4. Adaptive meshes generated by Algorithm 4.1 for $k = 0, 5, 10, 15$.

towards zero for increasing $k$, which is in agreement with Theorems 5.2 and 5.3. Also, a reliable prediction of the error by the estimator is confirmed by the efficiency index of about 5. Nonetheless, differently from the first example, we monitor a lower experimental order of convergence. This behavior is not surprising due to the poor regularity and the non-smoothness detected in the solution. Lastly, Table 5 provides the convergence history for the uniform mesh refinement strategy. It is notable that the adaptive method exhibits a significantly better numerical performance. In particular, by comparing the last rows in Tables 4 and 5, the accuracy of the adaptive method with a less number of DoF turns out to be 21 times better than the uniform mesh refinement strategy.

Based on the previous two numerical tests, we may safely conclude a reasonable numerical performance of Algorithm 4.1. In particular, the newly proposed adaptive algorithm seems to be competitive for dealing with the possible non-smoothness and

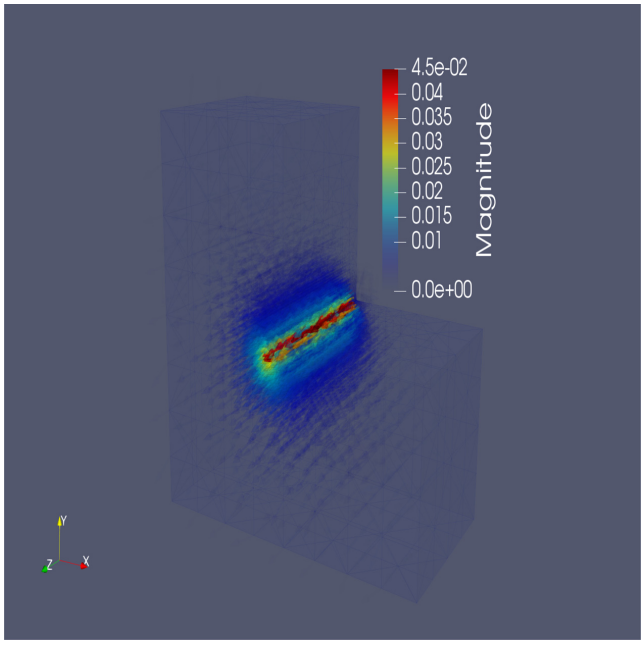


Fig. 5. Computed solution $\boldsymbol{u}_{15}$ on the finest adaptive mesh.

Table 4. Convergence history for the adaptive mesh refinement method.

| $k$ | DoF | $\|\boldsymbol{u}_{\text{ref}} - \boldsymbol{u}_k\|_{\boldsymbol{H}(\mathbf{curl})}$ | $\eta_k(\boldsymbol{u}_k, \boldsymbol{f}, g)$ | $\text{I}_k$ | $\text{ERC}_k$ |
|---|---|---|---|---|---|
| 10 | 20698 | 0.035612 | 0.173881 | 4.88268 | — |
| 11 | 45099 | 0.023059 | 0.112236 | 4.86727 | 0.124690 |
| 12 | 120536 | 0.016823 | 0.079759 | 4.74110 | 0.126012 |
| 13 | 274592 | 0.011287 | 0.060594 | 5.36816 | 0.237656 |
| 14 | 594234 | 0.007092 | 0.047992 | 6.76737 | 0.512425 |

Table 5. Convergence history for the uniform mesh refinement strategy.

| DoF | $\|\boldsymbol{u}_{\text{ref}} - \boldsymbol{u}_k\|_{\boldsymbol{H}(\mathbf{curl})}$ | $\text{ERC}_k$ |
|---|---|---|
| 1700 | 1.053573 | — |
| 12136 | 0.279670 | 0.674790 |
| 91472 | 0.194514 | 0.179768 |
| 709792 | 0.157557 | 0.102842 |

singularities in the solution of the nonlinear saddle point magnetostatic Maxwell system (1.1).

## 7. Concluding Remarks

We have derived an adaptive edge element method for the numerical solution of the quasilinear saddle point magnetostatic Maxwell system (1.1). Our main theoretical results include the establishment of the reliability and efficiency of the error estimator (3.1)–(3.3) and the $\boldsymbol{H}(\mathbf{curl})$-strong convergence of the discrete solutions generated by the new adaptive Algorithm 4.1. Numerical tests have confirmed these theoretical findings. Our future efforts may include the extension of the adaptive method to some other related problems, such as the optimal control problem associated with the system (1.1) and the nonlinear hyperbolic evolution Maxwell equations, which are truly challenging and related to many real-world applications, such as those in high-temperature superconductivity (see Refs. 43 and 44) and electromagnetic shielding (Ref. 45).

## Acknowledgments

The work of Yifeng Xu was partially supported by Natural Science Foundation of Shanghai (Projects 17ZR1420800 and 20JC1413800). The work of Irwin Yousept was supported by the German Research Foundation Priority Program DFG SPP 1962 "Non-smooth and Complementarity-based Distributed Parameter Systems: Simulation and Hierarchical Optimization", Project YO 159/2-2. The work of Jun Zou was substantially supported by Hong Kong RGC General Research Fund (Projects 14306719 and 14304517) and NSFC/Hong Kong RGC Joint Research Scheme 2016/17 (Project N_CUHK437/16).

## References

1. M. Ainsworth and J. T. Oden, *A Posteriori Error Estimation in Finite Element Analysis*, Pure and Applied Mathematics (Wiley-Interscience, 2000).
2. I. Babuška and W. Rheinboldt, Error estimates for adaptive finite element computations, *SIAM J. Numer. Anal.* **15** (1978) 736–754.
3. F. Bachinger, U. Langer and J. Schöberl, Numerical analysis of nonlinear multiharmonic eddy current problems, *Numer. Math.* **100** (2005) 593–616.
4. F. Bachinger, U. Langer and J. Schöberl, Efficient solvers for nonlinear time-periodic eddy current problems, *Comput. Vis. Sci.* **9** (2006) 197–207.
5. I. Babuška and M. Vogelius, Feedback and adaptive finite element solution of one-dimensional boundary value problem, *Numer. Math.* **44** (1984) 75–102.
6. R. Beck, R. Hiptmair, R. H. W. Hoppe and B. Wohlmuth, Residual based *a posteriori* error estimators for eddy current computation, *ESAIM Math. Model. Numer. Anal.* **34** (2000) 159–182.
7. L. Belenki, L. Diening and C. Kreuzer, Optimality of an adaptive finite element method for the $p$-Laplacian equation, *IMA J. Numer. Anal.* **32** (2012) 484–510.
8. C. Carstensen, M. Feischl, M. Page and D. Praetorius, Axioms of adaptivity, *Comp. Math. Appl.* **67** (2014) 1195–1253.

9. Z. Chen, L. Wang and W. Zheng, An adaptive multilevel method for time-harmonic Maxwell equations with singularities, *SIAM J. Sci. Comput.* **29** (2007) 118–138.
10. L. Chen and Y. Wu, Convergence of adaptive mixed finite element methods for Hodge Laplacian equation: Without harmonic forms, *SIAM J. Numer. Anal.* **55** (2017) 2905–2929.
11. J. Chen, Y. Xu and J. Zou, An adaptive edge element method and its convergence for a saddle-point from magnetostatics, *Numer. Meth. PDE* **28** (2012) 1643–1666.
12. P. G. Ciarlet, *Finite Element Methods for Elliptic Problems* (North-Holland, 1978).
13. P. Ciarlet, Jr., H. Wu and J. Zou, Edge element methods for Maxwell's equations with strong convergence for Gauss' laws, *SIAM J. Numer. Anal.* **52** (2014) 779–807.
14. P. Ciarlet, Jr. and J. Zou, Finite element convergence for the Darwin model to Maxwell's equations, *ESAIM Math. Model. Numer. Anal.* **31** (1997) 213–250.
15. P. Ciarlet, Jr. and J. Zou, Fully discrete finite element approaches for time-dependent Maxwell's equations, *Numer. Math.* **82** (1999) 193–219.
16. M. Costabel, M. Dauge and S. Nicaise, Singularities of Maxwell interface problems, *ESAIM: Math. Model. Numer. Anal.* **33** (1999) 627–649.
17. M. Costabel and M. Dauge, Singularities of electromagnetic fields in polyhedral domains, *Arch. Rational Mech. Anal.* **151** (2000) 221–276.
18. L. Diening and C. Kreuzer, Linear convergence of an adaptive finite element method for the $p$-Laplacian equation, *SIAM J. Numer. Anal.* **46** (2008) 614–638.
19. W. Dörfler, A convergent adaptive algorithm for Poisson's equation, *SIAM J. Numer. Anal.* **33** (1996) 1106–1124.
20. H. Duan, F. Qiu, Roger C. E. Tan and W. Zheng, An adaptive FEM for a Maxwell interface problem, *J. Sci. Comput.* **67** (2016) 669–704.
21. K. Eriksson and C. Johnson, Adaptive finite element methods for parabolic problems I: A linear model problem, *SIAM J. Numer. Anal.* **28** (1991) 43–77.
22. E. M. Garau, P. Morin and C. Zuppa, Convergence of an adaptive Kačanov FEM for quasi-linear problems, *Appl. Num. Math.* **61** (2011) 512–529.
23. E. M. Garau, P. Morin and C. Zuppa, Quasi-optimal convergence rate of an AFEM for quasi-linear problems of monotone type, *Numer. Math. TMA* **5** (2012) 131–156.
24. V. Girault and P. A. Raviart, *Finite Element Methods for Navier–Stokes Equations* (Spring-Verlag, 1986).
25. R. H. W. Hoppe and J. Schöberl, Convergence of adaptive edge element methods for the 3D currents equations, *J. Comput. Math.* **27** (2009) 657–676.
26. R. H. W. Hoppe and I. Yousept, Adaptive edge element approximation of $\boldsymbol{H}(\mathbf{curl})$-elliptic optimal control problems with control constraints, *BIT* **55** (2015) 255–277.
27. R. Hiptmair, Finite elements in computational electromagnetism, *Acta Numer.* **11** (2002) 237–339.
28. B. Kaltenbacher, M. Kaltenbacher and S. Reitzinger, Identification of nonlinear $\boldsymbol{B}$-$\boldsymbol{H}$ curves based on magnetic field computations and multigrid methods for ill-posed problems, *Eur. J. Appl. Math.* **14** (2003) 15–38.
29. I. Kossaczky, A recursive approach to local mesh refinement in two and three dimensions, *J. Comp. Appl. Math.* **55** (1995) 275–288.
30. A. Logg, K.-A. Mardal and G. N. Wells, *Automated Solution of Differential Equations by the Finite Element Method* (Springer, 2012).
31. P. Morin, K. G. Siebert and A. Veeser, A basic convergence result for conforming adaptive finite elements, *Math. Mod. Meth. Appl. Sci.* **18** (2008) 707–737.
32. J. Nédélec, Mixed finite elements in $\mathbb{R}^3$, *Numer. Math.* **35** (1980) 315–341.

33. R. H. Nochetto, K. G. Siebert and A. Veeser, Theory of adaptive finite element methods: An introduction, in *Multiscale, Nonlinear and Adaptive Approximation*, eds. R. A. DeVore and A. Kunoth (Springer, 2009), pp. 409–542.
34. B. Scheurer, Existence et approximation de points selles pour certains problèmes nonlinéaires, *RAIRO Anal. Numér.* **11** (1977) 369–400.
35. J. Schöberl, *A posteriori* error estimates for Maxwell equations, *Math. Comp.* **77** (2008) 633–649.
36. L. R. Scott and S. Zhang, Finite element interpolation of nonsmooth functions satisfying boundary conditions, *Math. Comp.* **54** (1990) 483–493.
37. K. G. Siebert, A convergence proof for adaptive finite elements without lower bounds, *IMA J. Numer. Anal.* **31** (2011) 947–970.
38. C. Traxler, An algorithm for adaptive mesh refinement in $n$ dimensions, *Computing* **59** (1997) 115–137.
39. A. Veeser, Convergent adaptive finite elements for the nonlinear Laplacian, *Numer. Math.* **92** (2002) 743–770.
40. R. Verfürth, *A Posteriori Error Estimation Techniques for Finite Element Methods* (Oxford University Press, 2013).
41. Y. Xu and J. Zou, A convergent adaptive edge element method for an optimal control problem in magnetostatics, *ESAIM: Math. Model. Numer. Anal.* **51** (2017) 615–640.
42. I. Yousept, Optimal control of quasilinear $\boldsymbol{H}(\mathbf{curl})$-elliptic partial differential equations in magnetostatic field problems, *SIAM J. Control Optim.* **51** (2013) 3624–3651.
43. I. Yousept, Optimal control of non-smooth hyperbolic evolution Maxwell equations in type-II superconductivity, *SIAM J. Control Optim.* **55** (2017) 2305–2332.
44. I. Yousept, Hyperbolic Maxwell variational inequalities of the second kind, *ESAIM: Control Optim. Calc. Var.* **26** (2020) 34.
45. I. Yousept, Well-posedness theory for electromagnetic obstacle problems, *J. Differential Equations* **269** (2020) 8855–8881.
46. W. Zheng, L. Wang and Z. Chen, An adaptive element method for $\boldsymbol{H}$-$\psi$ formulation of time-dependent eddy current problems, *Numer. Math.* **103** (2006) 667–689.
47. L. Zhong, L. Chen, S. Shu, G. Wittum and J. Xu, Convergence and optimality of adaptive edge finite element methods for time-harmonic Maxwell equations, *Math. Comp.* **81** (2012) 623–642.